NLRP3 inflammasome priming and activation are regulated by a novel phosphatidylinositol-dependent mechanism

Claire Hamilton[1,#], Antoni Olona[1,#], Stuart Leishman[1], Kelly MacDonald-Ramsahai[1], Shamshad Cockcroft[2], Gerald Larrouy-Maumus[3], and Paras K. Anand[1,]*

[1]Department of Infectious Disease, Imperial College London, London, W12 0NN, UK.

[2]Department of Neuroscience, Physiology and Pharmacology, Division of Biosciences, University College London, London WC1E 6JJ, UK.

[3]MRC Centre for Molecular Bacteriology and Infection, Department of Life Sciences, Imperial College London, London, SW7 3AZ, UK.

***Corresponding author**

E-mail: Paras.Anand@imperial.ac.uk (PKA)

# These authors contributed equally

Running Title: PI acyl chains regulate NLRP3 activation.

Keywords: NLRP3, Lipid homeostasis, Inflammasome, Phosphatidylinositol, TIRAP

Summary

Imbalance in lipid homeostasis is associated with discrepancies in immune signalling and is tightly linked to metabolic disorders. The diverse ways in which lipids impact immune signalling, however, remain ambiguous. The phospholipid phosphatidylinositol (PI), which is implicated in numerous immune disorders, is chiefly defined by its phosphorylation status. By contrast, the significance of the two fatty acid chains attached to the PI remains unknown. Here, by employing a mass-spectrometry-based assay, we demonstrate a role for PI acyl group chains in regulating both the priming and activation steps of the NLRP3 inflammasome in mouse macrophages. In response to NLRP3 stimuli, cells deficient in ABC transporter ABCB1, which effluxes lipid derivatives, revealed defective inflammasome activation. Mechanistically, *Abcb1*-deficiency shifted the total PI configuration exhibiting a reduced ratio of short-chain to long-chain PI-acyl lipids. Consequently, *Abcb1*-deficiency resulted in rapid degradation of TIRAP, the TLR adaptor protein which binds PI(4,5)-phosphate. Moreover, this accompanied increased NLRP3 phosphorylation at the Ser293 position and blunted inflammasome activation. Exogenously supplementing WT cells with linoleic acid, but not arachidonic acid, reconfigured PI acyl chains. Accordingly, linoleic acid supplementation increased TIRAP degradation, elevated NLRP3 phosphorylation, and abrogated inflammasome activation. Altogether, our study reveals a novel metabolic-inflammatory circuit which contributes to calibrating immune responses.

45 **Introduction**

46 The NLRP3 inflammasome is a multiprotein complex activated in response to diverse
47 pathogen-associated and 'danger' signals, and plays important roles during infectious and
48 inflammatory diseases (Lupfer and Anand, 2016; Man and Kanneganti, 2015). The activation
49 of NLRP3 inflammasome involves two steps in which NLRP3 is first licensed downstream of
50 TLR signalling. This step, also known as the priming step, has both NF-κB-dependent and -
51 independent consequences during NLRP3 activation. Upon sensing an apt stimulus, NLRP3
52 complexes with pro-caspase-1 and the adaptor molecule ASC. Consequently, caspase-1 is
53 activated by auto-proteolysis, which further results in the maturation and release of biologically
54 active forms of cytokines IL-1β and IL-18. Additional regulation is mediated by the post-
55 translational modification of distinct NLRP3 domains which may affect either the priming or
56 activation of the NLRP3 inflammasome (Lopez-Castejon et al., 2013; Yang et al., 2017).
57 Inflammasome activation also results in the induction of inflammatory form of cell death,
58 pyroptosis, by a Gasdermin-D-dependent mechanism (Kayagaki et al., 2015). Recent studies
59 have revealed elaborate links between lipid metabolism and inflammasome activation (Anand,
60 2020). We, and others, previously demonstrated vital roles for cholesterol biosynthesis and
61 transport in NLRP3 inflammasome activation (de la Roche et al., 2018; Guo et al., 2018).
62 Other recent studies have demonstrated that NLRP3 recruitment to the dispersed *trans*-Golgi
63 network requires binding to phosphoinositide 4-phosphate (PI4P) prior to NLRP3 activation
64 (Chen and Chen, 2018). The mechanisms of NLRP3 inflammasome activation and,
65 remarkably, the roles lipids play in the process remain ambiguous.

66 Lipid homeostasis is critical to all physiological processes including immune signalling (Barnett
67 and Kagan, 2020). Lipids form the structural framework which imparts fluidity to membranes.
68 Driven by their amphipathic nature, membrane lipids enable compartmentalization of cellular
69 constituents both from the outside environment, and into discrete organelles (Casares et al.,
70 2019). The lipid composition of membranes, in addition, is pivotal in shaping the localization,
71 conformation, and thus the activity of lipid-protein and protein-protein complexes (Fernandis

72 and Wenk, 2007). The latter is fundamental to cellular signalling emanating from the
73 cholesterol-rich membrane-microdomains which serve as signalling platforms and are the
74 preferred sites for pathogen entry (Kaul et al., 2004). Additionally, phosphoinositides (PIPs),
75 the phosphorylated derivatives of the parent phosphatidylinositol (PI), play important roles in
76 immune signalling by ensuring precise recruitment of the adaptor protein TIRAP, also known
77 as Mal, to the activated TLRs at the plasma and endosomal membranes (Kagan and
78 Medzhitov, 2006). Structurally, PI consists of an inositol head group and two fatty acyl chains
79 linked by a glycerol backbone (Goud et al., 2016). The binding of PIPs to the phosphoinositide-
80 binding domain of TIRAP results in the recruitment of MyD88 and the IRAK family of kinases
81 to activated TLRs thereby promoting downstream NF-kB activation. Accordingly, the
82 synthesis, turnover, and localization of PIPs may influence TLR-dependent signalling.

83 Homeostasis of the cellular lipid composition is largely maintained by the SREBP family of
84 transcription factors that transcribe genes involved in lipid uptake, biosynthesis, and efflux
85 (Horton et al., 2002). When in excess, lipids are either stored in the form of lipid droplets or
86 are effluxed by the activity of the ABC family of transporters. The family members ABCA1 and
87 ABCG1 facilitate cholesterol efflux to apolipoproteins and HDL, respectively (Yvan-Charvet et
88 al., 2010). Moreover, deficiency in ABCA1 and ABCG1 is associated with enhanced secretion
89 of inflammatory mediators, including IL-1β (Westerterp et al., 2017). Correspondingly, the
90 efflux transporters play anti-inflammatory functions in diverse diseases (He et al., 2020; Sonett
91 et al., 2018) suggesting a possible link between lipid metabolism and immune signalling
92 (Castrillo et al., 2003). Cells deficient in *Abca1* and *Abcg1* cannot unload surplus lipids
93 exhibiting elevated cholesterol accumulation which, independently, improves cytokine
94 secretion (Westerterp et al., 2017; Yvan-Charvet et al., 2010). Overall, this argues that
95 immune signalling is profoundly determined by lipid metabolism, but cholesterol accumulation
96 remains a confounding factor and detailed mechanisms remain poorly defined. In this study,
97 we investigated the role of lipid metabolism in immune signalling by studying ABCB1. ABCB1
98 (or P-glycoprotein) is a well-characterized family member that imparts multi-drug resistance to

99 malignant cells but has no impact on cellular cholesterol levels (To et al., 2014; Vaidyanathan
100 et al., 2016). The precise functions of ABCB1 in inflammasome activation remain undefined.

101 Here, we demonstrate a role for ABCB1 and PI fatty acyl chains in regulating the NLRP3
102 inflammasome. Mechanistically, *Abcb1*$^{-/-}$ cells displayed a reduced ratio of short-chain to long-
103 chain PI acyl chain lipids. This change in PI configuration was independent of the expression
104 of enzymes that both synthesize PI and are involved in acyl chain remodelling. Remarkably,
105 the shift in acyl chain composition regulated both NLRP3 priming and activation steps: it
106 resulted in the depletion of TLR adaptor protein, TIRAP, and additionally elevated
107 phosphorylation in the NACHT domain of NLRP3. Intriguingly, exogenously supplementing
108 WT cells with linoleic acid reconfigured PI acyl chains, which accordingly mimicked *Abcb1*-
109 deficient cells in TIRAP depletion, NLRP3 phosphorylation, and blunted inflammasome
110 activity. Our study thus identifies an important role for PI lipid chain configuration in modulating
111 inflammasome activity which may have significant implications in metabolic diseases.

112

113 **Results**

114 **ABC transporter B family member 1 is required for caspase-1 activation and IL-1β**
115 **secretion.**

116 Lipids are involved in diverse functions including maintenance of membrane structure, cellular
117 signalling, and immunity (Barnett and Kagan, 2020; Casares et al., 2019). Consequently,
118 altered lipid levels can lead to metabolic and inflammatory disorders, or may result in
119 lipotoxicity (Sonett et al., 2018). Therefore, lipid homeostasis, and in particular, lipid efflux, is
120 critical to normal cell function. Members of the ABC family function to export substrates, mainly
121 lipids and related molecules, out of the cytosol (Yvan-Charvet et al., 2010). For example,
122 ABCA1 is primarily associated with phospholipid and cholesterol transport to lipid-poor ApoA-
123 I, while ABCG1 exports cholesterol to more mature HDL particles. Remarkably, deficiency in
124 *Abca1* and *Abcg1* results in elevated secretion of inflammatory mediators in response to

125 pathogenic stimuli (Westerterp et al., 2017). To address the roles of lipid metabolism in
126 immune signalling, we investigated the role of ABCB1 in inflammasome activation. ABCB1
127 alters lipid metabolism and has a broad substrate specificity in transporting a range of drugs
128 (Romsicki and Sharom, 2001). However, the transporter does not affect overall cellular lipid
129 or cholesterol levels.

130 In order to test the role ABCB1 plays in inflammasome activation, we generated genetic knock-
131 out cell lines using the CRISPR/Cas9 approach in immortalised bone marrow-derived
132 macrophages (iBMDMs). In contrast to humans where a single isoform of ABCB1 is
133 expressed, the mouse genome expresses two isoforms, *Abcb1a* and *Abcb1b* (Kalabis et al.,
134 2005). We first examined the expression of the two isoforms in bone-marrow-derived mouse
135 macrophages. PCR amplification followed by gel electrophoresis revealed that both *Abcb1a*
136 and *Abcb1b* are expressed in unstimulated and LPS-stimulated iBMDMs **(Fig. S1A and S1B)**.
137 However, quantitative PCR revealed that *Abcb1b* is expressed at approximately 600-fold
138 higher levels than that of *Abcb1a*, suggesting that this isoform predominates in mouse
139 macrophages **(Fig S1C)**. Similar results were obtained with primary mouse macrophages **(Fig**
140 **S1D** and data not shown**)**. Additionally, the expression of *Abcb1b* was only marginally higher
141 in LPS-stimulated macrophages compared to control cells at all time-points tested, though
142 there was a slight initial decrease in expression upon LPS stimulation **(Fig S1E)**. These
143 studies, therefore, suggest a potential role for ABCB1 in immune cells.

144 Two cell lines, *Abcb1b*$^{-/-}$ #1 and #2, were established with deletions in exon 10 of the protein,
145 as verified by Sanger sequencing **(Fig S1F)**. The mRNA expression of *Abcb1b* in the two
146 CRISPR cell lines was reduced significantly though the PCR amplicon was still synthesized to
147 some extent **(Fig S1G)**. However, compared to WT cells, the protein expression of ABCB1
148 was diminished by more than 70% and 90% in the two cell lines potentially suggesting the
149 presence of unstable mRNA in edited cell lines **(Figs 1A and 1B)**.

150 To test the activity of ABCB1 in edited cells, we made use of Rhodamine 123 (Rho123) dye.
151 Rho123 passively diffuses across biological membranes but is subsequently metabolised by

152 intracellular esterases to yield a fluorescent compound that has reduced permeability (Forster
153 et al., 2012). The efflux of the dye out of cells requires active transport by ABCB1 and certain
154 other ABC transporters (Forster et al., 2012). *Abcb1*$^{-/-}$ cells exposed for 30 min to Rho123
155 showed increased sequestration of the dye compared to control cells thereby confirming
156 inhibition of ABCB1 transporter activity **(Fig 1C)**.

157 Unlike other ABC transporters that are involved in lipid efflux, ABCB1 is not known to alter
158 cellular cholesterol levels (Garrigues et al., 2002). In agreement, WT and *Abcb1b*$^{-/-}$
159 macrophages exhibited no qualitative differences in cholesterol esterification upon staining
160 with filipin, a compound that binds to free unesterified cholesterol (de la Roche et al., 2018).
161 Excitation of filipin by UV fluorescence showed no obvious differences in either the levels or
162 distribution of cholesterol between WT and *Abcb1b*$^{-/-}$ cells **(Fig 1D)**. As a control, we exposed
163 WT cells to U18666a, which specifically blocks the lysosomal cholesterol transporter, NPC1
164 (de la Roche et al., 2018), and this resulted in expected punctate filipin staining suggestive of
165 lysosomal cholesterol accumulation **(Fig 1D)**. Additionally, quantitative analysis of total cellular
166 cholesterol revealed similar levels in both WT and *Abcb1b*$^{-/-}$ cells **(Fig 1E)**. These data agree
167 with previous studies and indicate no major effect of ABCB1 deficiency on cholesterol
168 esterification, distribution, and efflux.

169 We next tested the activation of NLRP3 inflammasome in macrophages with genetic deletion
170 of *Abcb1b*. WT and *Abcb1*$^{-/-}$ cells were exposed to LPS for 4h followed by either ATP or
171 nigericin. NLRP3 inflammasome activation results in the assembly of the inflammasome
172 complex containing NLRP3, the adaptor ASC, and pro-caspase-1. Pro-caspase-1 is then
173 cleaved into its active p20 form, which subsequently results in the maturation and secretion of
174 pro-inflammatory cytokines, IL-1β and IL-18. Compared to WT cells, *Abcb1b*$^{-/-}$ cells exhibited
175 diminished caspase-1 cleavage and IL-1β secretion upon exposure to both nigericin and ATP
176 **(Figs 1F and 1G)**. Activation of the NLRP3 inflammasome also leads to an inflammatory form
177 of cell death, termed pyroptosis, which is mediated by gasdermin-D (GSDMD). Cleavage of
178 GSDMD by caspase-1 results in an N-terminal fragment, which subsequently polymerises and

179 forms pores in the cell membrane, ultimately leading to cell rupture. GSDMD cleavage in
180 *Abcb1b*$^{-/-}$ macrophages was diminished in comparison to WT cells following NLRP3
181 inflammasome activation, further corroborating reduced caspase-1 in deficient cells **(Fig 1F)**.

182 We next used elacridar, a third-generation inhibitor, that has been shown to inhibit ABCB1
183 activity and overcome drug resistance in cancer models (Dash et al., 2017). Primary BMDMs
184 treated overnight with increasing concentrations of elacridar and exposed for 30 min to
185 Rho123 exhibited increased sequestration of the dye compared to control cells **(Fig 1H)**. In
186 agreement with deficient cells, treatment of WT macrophages with increasing concentrations
187 of elacridar followed by NLRP3 activation resulted in a dose-dependent decrease in the
188 generation of cleaved caspase-1 p20 form **(Fig 1I)**, and reduction in IL-1β and IL-18 secretion
189 **(Figs 1J and 1K)**. Similar results were observed with the $P2X_7$ receptor agonist and NLRP3
190 activator, ATP **(Figs S2A and S2B, and Fig 1K)**. Together, these data demonstrate the
191 functional requirement of ABCB1 in NLRP3 inflammasome activation.

192

193 **ABCB1 is required for the priming and activation of the NLRP3 inflammasome.**

194 NLRP3 inflammasome activation requires two distinct steps. The priming step results in the
195 induction of TLR-dependent NF-κB activation, which in turn leads to the transcriptional and
196 translational upregulation of NLRP3 and pro-IL-1β. The second signal activates the NLRP3
197 inflammasome complex, leading to caspase-1 activation (Hamilton et al., 2017; Hamilton and
198 Anand, 2019). We next studied the precise step at which ABCB1 is required for activation of
199 the NLRP3 inflammasome by examining the expression of inflammasome components
200 including NLRP3, and pro-IL-1β. Stimulation with LPS and ATP upregulated the NLRP3 and
201 pro-IL-1β protein in WT cells, which was found to be blunted in cells lacking *Abcb1* **(Fig 2A)**.
202 By contrast, pro-caspase-1 and ASC are constitutively expressed, and their expression
203 remained unaltered in *Abcb1b*$^{-/-}$ macrophages **(Figs 1F and 2A)**. These results coincided with
204 reduced upregulation of *Nlrp3* and *Il1b* at the mRNA level **(Figs 2B and 2C)**.

205 NF-κB is inactive within the cell prior to stimulation through binding to the inhibitory protein
206 IκB. Upon TLR stimulation, signal transduction leads to the activation of the IKK complex,
207 which subsequently phosphorylates IκB, targeting it for degradation. This allows NF-κB to
208 translocate to the nucleus and initiate gene transcription. In addition to NF-κB activation, TLR
209 stimulation also leads to the activation of MAPKs, notably p38 (Kawasaki and Kawai, 2014).
210 In agreement with the above data, the phosphorylation of IκB and p38 MAPK was reduced in
211 LPS-stimulated *Abcb1b*$^{-/-}$ cells compared to WT cells **(Fig 2D)**. We also examined the
212 expression of other NF-κB -dependent cytokines and chemokines in response to TLR4
213 activation and their expression were similarly decreased in cells lacking ABCB1 **(Figs 2E-G)**.
214 Moreover, the mRNA expression of interferon-β, which is dependent on adaptor TRIF upon
215 LPS stimulation, was also reduced in *Abcb1b*$^{-/-}$ cells **(Fig 2H)**. Furthermore, this response
216 was not specific to TLR4 ligation, as activation of TLR2 or TLR7 by Pam3CSK4 and
217 imiquimod, respectively also resulted in diminished upregulation of *Nlrp3, Il1β, Tnfα* and *Cxcl1*
218 (KC) mRNA expression **(Fig 2I, and Figs S3A-C)**. These data suggested blunted TLR-
219 dependent signalling in the absence of ABCB1.

220

221 **ABCB1 does not affect the activation of NLRC4 and AIM2 inflammasomes.**

222 We next tested the requirement of ABCB1 during NLRC4 and AIM2 inflammasome activation.
223 Unlike NLRP3, the expression of NLRC4 and AIM2 is constitutively expressed at significantly
224 higher levels in mouse macrophages. However, the expression and therefore the secretion of
225 downstream effector cytokine IL-1β still requires upregulation by TLR signalling. Activation of
226 NLRC4 inflammasome by *Salmonella* infection and AIM2 inflammasome by exposure to
227 poly(dA:dT) resulted in comparable caspase-1 cleavage between WT and *Abcb1b*$^{-/-}$ cells **(Fig**
228 **3A** and data not shown). However, the levels of IL-1β secretion, as expected, were found
229 diminished in both *Abcb1b*$^{-/-}$ cells and in WT cells where ABCB1 was pharmacologically
230 blocked during NLRC4 and AIM2 inflammasome activation **(Figs 3B and 3C)**. In contrast to

231 pro-IL-1β, pro-IL-18 is constitutively expressed and does not require TLR signalling for
232 upregulation. In agreement, no difference in IL-18 production was observed following NLRC4
233 or AIM2 inflammasome activation in cells lacking ABCB1 **(Fig 3D)**. Secretion of IL-18,
234 however, following NLRP3 activation showed complete abolishment in *Abcb1b*$^{-/-}$ macrophages
235 **(Fig 3D)**. These data suggest that the function of ABCB1 is specific to the NLRP3
236 inflammasome, and that the diminished IL-1β production is due to dampened NF-κB signalling
237 in *Abcb1b*$^{-/-}$ cells **(Figs 2C and 2D)**.

238

239 **Blunted NLRP3 inflammasome activation is associated with a shift in PI lipid chains.**

240 A notable feature of the plasma membrane is the distinct lipid composition in the two leaflets
241 of the bilayer (Van Meer et al., 2008). Sphingolipids are mostly present in the outer leaflet
242 while glycerophospholipids such as phosphatidylethanolamine (PE), phosphatidylserine (PS),
243 and phosphatidylinositol (PI) are mostly restricted to the inner leaflet thereby imparting distinct
244 functions to the membranes (Van Meer et al., 2008).

245 To further investigate the mechanism by which *Abcb1*-deficiency dampens NLRP3 activation,
246 we performed whole-cell lipidomics by MALTI-TOF MS. Our experiments revealed ions in the
247 800 – 1700 *m/z* range. The most striking change was observed in the 800-920 *m/z* range
248 which represents the total PI complement present in cells with distinct signals corresponding
249 to anticipated PI masses. In mammalian cells, a large fraction of the PIP molecules has
250 saturated stearic acid (18:0) at the *sn*-1 position and unsaturated arachidonic acid (20:4) at
251 the *sn*-2 position **(Fig 4A)**. Consequently, both the WT and *Abcb1*$^{-/-}$ cells exhibited a peak at
252 *m/z* 885.4, described together as PI (38:4) **(Figs 4B and 4C)**. Additionally, another PI peak at
253 *m/z* 861.4, corresponding to PI (36:2), was observed in WT and *Abcb1*$^{-/-}$ cells **(Figs 4B and**
254 **4C)**. MS/MS fragmentation of the peaks at *m/z* 861 and *m/z* 885 revealed the presence of
255 stearic acid, arachidonic acid, and oleic acid **(S4 Fig)**. Besides the presence of PIs with distinct
256 acyl chain lengths, other closely related PI siblings were also represented though at much

257 lower levels **(Figs 4B and 4C, and Fig S5)**. Notably, the WT cells exhibited almost equal
258 levels of the two PI-lipid masses at 861 and 885. By contrast, *Abcb1*-deficient cells favoured
259 higher levels of PI (38:4) compared to PI (36:2) which was expressed at significantly lower
260 levels. As a result, the ratio of the two PI-lipid masses consistently demonstrated a significant
261 difference between WT and *Abcb1*$^{-/-}$ cells **(Fig 4D)**. These studies, therefore, suggest that the
262 deficiency in *Abcb1* modifies the PI fatty acyl configuration resulting in a reduced ratio of short-
263 chain to long-chain fatty acids. **(Fig 4D)**.

264 Further analysis of the mass-spec data also unveiled several ganglioside peaks that were
265 distinct between WT and *Abcb1b*$^{-/-}$ macrophages. In particular, the percentage of GM1
266 ganglioside was significantly reduced in *Abcb1b*$^{-/-}$ cells **(Fig S6A)** which was further confirmed
267 qualitatively and quantitatively by labelling WT and *Abcb1*$^{-/-}$ cells with cholera toxin subunit B
268 (CTB) or by flow cytometry **(Figs S6B-F)**.

269 The *de novo* synthesis of PI occurs at the ER through the conversion of phosphatidic acid
270 (PA) via 2 enzymatic reactions **(Fig 4E)**. PA is first converted into an intermediate, cytidine
271 diphosphate-diacylglycerol (CDP-DAG), by CDP-DAG synthase (CDS). CDP-DAG is then
272 converted to PI by PI-synthase (also known as CDIPT) (Blunsom and Cockcroft, 2020; Le
273 Guédard et al., 2009). Cleavage of the fatty acid by phospholipases A, followed by acylation
274 by acyl-CoA–specific lysophospholipid acyltransferase enzymes, is needed to incorporate a
275 new fatty acid molecule (Barneda et al., 2019). Lysophosphatidylinositol acyltransferase
276 (LPIAT) has been shown to reacylate PI with polyunsaturated substrates such as arachidonic
277 acid, while lysocardiolipin acyltransferase 1 (LCLAT1) has been demonstrated to reacylate
278 with stearic acid (Barneda et al., 2019) **(Fig 4E)**. As *Abcb1b*-deficient macrophages displayed
279 altered PI lipid chains, we investigated whether this was due to a defect in PI synthesis and or
280 acyl chain remodelling. However, the mRNA expression of *Cds2* (*Cds1* was expressed with
281 Ct value >30) and *Cdipt* revealed no significant difference between WT and *Abcb1b*$^{-/-}$ cells
282 **(Figs 4F and 4G)**. Similarly, the mRNA expression of *Lclat1* and *Lpiat* remained unchanged
283 in deficient cells **(Figs 4H and 4I)**. These data indicate that ablation of *Abcb1* in macrophages

284 alters PI lipid chain configuration independently of the synthesis of PI or remodelling of its acyl
285 chain composition.

286

287 **Exogenous supplementation with linoleic acid alters PI acyl chain configuration.**

288 To further understand the mechanistic underpinnings of our findings and to validate them, we
289 next sought to identify the fatty acids which may alter PI acyl chains and subsequently modify
290 inflammasome activity. In agreement with previous studies (Hunt et al., 2004), we
291 hypothesized that exogenous supplementation with distinct fatty acids will alter cellular PI acyl
292 chain conformation. To achieve this, cells were grown for at least two weeks in growth media
293 supplemented with different fatty acids prior to validating the samples by mass spectrometry
294 **(Fig 5A)**. These assays revealed that prolonged supplementation with linoleic acid, but not
295 arachidonic acid, favoured long-chain fatty acids **(Fig 5A)**. This was predominantly reflected
296 in the increased concentration of unsaturated acyl chains at the *sn*-2 position. Compared to
297 control cells, supplementation with linoleic acid changed the fatty acid composition to that
298 observed in *Abcb1*$^{-/-}$ cells **(Figs 5A, S4, and S5)**. Consequently, these cells behaved similarly
299 to cells lacking ABCB1. Strikingly, supplementation with arachidonic acid did not result in any
300 noticeable difference **(Fig S5)**. Notably, we also observed a narrower range over which
301 macrophages tolerated arachidonic acid (data not shown). Accordingly, compared to control
302 cells, WT cells grown in the presence of linoleic acid demonstrated reduced *Nlrp3* and *Il-1β*
303 mRNA expression **(Figs 5B and 5C)**. Again, these results were specific for linoleic acid as
304 supplementation with arachidonic acid, alone or in combination with stearic acid, neither
305 altered the *m/z* 861/885 ratio nor the mRNA expression of *Nlrp3* and *Il-1β* **(Figs 5A, 5D and**
306 **5E, and S5)**. Furthermore, like *Abcb1*$^{-/-}$ cells, exogenous linoleic acid resulted in the disruption
307 of GM1 presence in WT cells **(Fig 5F and 5G)**. These results, therefore, demonstrate that
308 linoleic acid supplementation alters the PI acyl chain profile.

309

310 **PI acyl chain profile regulates TIRAP expression.**

311 TLRs are transmembrane receptors that can sense microbial products at distinct subcellular
312 sites. Ligation of TLRs at both the plasma membrane and endosomes triggers a signal
313 transduction pathway involving the adaptor protein MyD88 which is recruited to the conserved
314 TIR domain present in the cytosolic tails of these receptors. Most TLRs recruit MyD88 by
315 employing the intermediate sorting adaptor TIRAP, which is bound to either PIP2 or PI4P for
316 precise localization, and is prepositioned on the membranes prior to TLR activation. The
317 phosphorylation by Bruton's tyrosine kinase activates TIRAP but this is immediately followed
318 by SOCS1-mediated TIRAP polyubiquitination and degradation to avoid sustained signalling
319 (Mansell et al., 2006). The rapid turnover of TIRAP is similarly regulated by serine/threonine
320 kinases, interleukin-1 receptor-associated kinases IRAK1 and IRAK4, which directly
321 phosphorylate TIRAP triggering Lys48 -linked ubiquitination and proteasomal degradation
322 (Dunne et al., 2010).

323 We next evaluated the role of altered PI-acyl chain composition on TLR signalling by
324 assessing TIRAP expression. As reported in previous studies, we mostly found TIRAP at the
325 cell periphery with additional punctate staining in the cytoplasm **(Fig. 6A)**. Stimulation of WT
326 cells with LPS resulted in increased proximity of TIRAP to the plasma membrane **(Fig. 6A)**.
327 LPS stimulation resulted in a modest increase in TIRAP expression as observed by WB at 15
328 min followed by sustained TIRAP expression up to 60 min, the last time point that we tested
329 **(Fig. 6B and 6C)**. By contrast, cells lacking *Abcb1* or those exposed to linoleic acid, exhibited
330 significant depletion in TIRAP expression **(Fig. 6B and 6C)**. Following phosphorylation, TIRAP
331 is degraded by the 26S proteasome. Accordingly, pre-treatment of linoleic acid -supplemented
332 cells with the proteasomal inhibitor MG132 restored TIRAP expression **(Fig. 6C)**. These
333 studies, therefore, suggest that change in PI fatty acid configuration modifies TLR signalling
334 by regulating the degradation of adaptor protein TIRAP.

335

336 **Altered PI acyl chain profile blunts inflammasome activity by increasing NLRP3**
337 **phosphorylation.**

338 The NLRP3 inflammasome is regulated both at the transcriptional and post-translational
339 levels. In particular, NLRP3 phosphorylation at distinct sites regulates both the priming and
340 activation steps. Notably, linoleic acid derivative, prostaglandin E2, has been shown to
341 facilitate NLRP3 phosphorylation in the NACHT domain at Ser293 position (Ser295 in
342 humans) by inducing protein kinase A (Mortimer et al., 2016). Therefore, we next tested the
343 status of NLRP3 Ser293 phosphorylation in control and linoleic acid -supplemented cells. We
344 noted from different experiments that cells exposed to linoleic acid display on average 1.5
345 times less NLRP3 expression due to defective priming under these conditions. To ensure that
346 we examined phosphorylation on equal NLRP3 protein levels, we increased the amount of
347 protein loaded onto gels in linoleic acid -supplemented cell lysates. Accordingly, increasing
348 the protein concentration by the above fraction resulted in similar total NLRP3 expression in
349 both control and linoleic acid-supplemented samples **(Fig. 7A)**. By contrast, compared to
350 control cells, linoleic acid-exposed cells demonstrated increased phosphorylation as
351 examined using a phospho-NLRP3 specific antibody **(Fig. 7A and 7B)**. In agreement, linoleic
352 acid -supplemented cells exhibited reduced caspase-1 activity **(Fig. 7C)**. However, exposure
353 to arachidonic acid resulted in similar caspase-1 activity **(Fig. 7C).** Moreover, linoleic acid
354 supplementation diminished the secretion of IL-18 from LPS-primed cells in response to both
355 ATP and nigericin **(Fig. 7D)**. In order to further validate our results, we next examined
356 inflammasome assembly by examining ASC speck formation. NLRP3 inflammasome
357 activation by LPS+ATP resulted in a comparable percentage of ASC specks in both control
358 WT and cells exposed to arachidonic acid **(Fig. 7E and 7F)**. By comparison, cells lacking
359 *Abcb1* exhibited significantly reduced ASC specks. Similarly, cells grown in linoleic acid-rich
360 media displayed reduced ASC speck formation **(Fig. 7E and 7F)**. Together, these data
361 demonstrate that altered PI acyl chain configuration affects both the priming and activation
362 steps of the NLRP3 inflammasome.

363

364 **Discussion**

365 Our studies described here demonstrate that lipid metabolism is intricately linked to immune
366 signalling and inflammasome activation. Genetic or pharmacological depletion of ABCB1
367 abolished caspase-1 cleavage and IL-1β secretion. Remarkably, this was restricted to the
368 NLRP3 inflammasome as *Abcb1*$^{-/-}$ cells displayed comparable activation of the NLRC4 and
369 AIM2 inflammasomes. Further mechanistic studies based on whole-cell lipidomics revealed
370 an altered PI lipid chain profile in deficient cells. Remarkably, modified PI lipid chain
371 configuration accompanied reduced TIRAP expression and altered NLRP3 phosphorylation;
372 together they affected both NLRP3 inflammasome priming and activation steps **(Fig. 8)**.
373 Notably, prolonged growth in media supplemented with linoleic acid reconfigured PI acyl chain
374 profile in WT cells thereby mimicking the phenotypic features observed in deficient cells
375 including aberrant inflammasome activity. Our results, therefore, demonstrate the metabolic
376 regulation of inflammasome activation by PI acyl chains.

377 PIPs, which take key roles in membrane trafficking and signal transduction, are defined by the
378 phosphorylation of their inositol head group (Dickson and Hille, 2019; Falkenburger et al.,
379 2010). By contrast, the significance of the attached fatty acids has remained unappreciated
380 (Barneda et al., 2019; Traynor-Kaplan et al., 2017). In mammalian cells, approximately 40-
381 80% of the PIP molecules contain stearoyl/arachidonyl in the *sn*-1 and *sn*-2 positions,
382 respectively designated as C18:0/C20:4 or 38:4 for the complete molecule (Falkenburger et
383 al., 2010). A previous study revealed that mutations in the *p53* gene expand PIs containing
384 short-length acyl chains, corresponding to 36-carbon PIs (Naguib et al., 2015). Remarkably,
385 the shift in PI-lipids was not reflected in the lipid spectra of phosphatidylcholine (PC), asserting
386 that the modification is not distinctive of all phospholipids (Naguib et al., 2015). Notably, both
387 PC and PI share a common precursor, phosphatidic acid (PA). However, the latter steps in
388 the pathway involve distinct enzymes to generate either PI or PC. Our studies revealed that
389 *Abcb1*-deficient cells expressed comparable levels of PI synthase as well as the enzymes

390 involved in PI acyl chain remodelling thus excluding these as a probable reason. As a result,
391 it remains unclear as to how *Abcb1*-deficient cells acquire a distinct composition of PI-lipid
392 chains. It is tempting to speculate that the precursor PA possessing a different lipid content
393 gets accumulated in distinct membranes which is spatially only accessible to PI enzymes in
394 deficient cells. Alternatively, it is also possible that the mature PIs are able to remodel their
395 lipid chains once they have formed. If true, it will be interesting to decipher the mechanisms
396 that prompt this variation.

397 Our study suggests that ABCB1 is critical in retaining immune equilibrium and the loss of
398 ABCB1 dampens inflammasome activation. Keeping in view that aberrant PI signalling
399 (including by the PI3K/AKT pathway) is associated with malignancies, it is plausible that
400 ABCB1 does not exclusively regulates PI-lipid profile, and there exists redundancy in this
401 pathway acting as a fail-safe mechanism. Accordingly, supplementation with linoleic acid
402 similarly altered the PI profile incorporating elevated arachidonic acid levels. Notably, this
403 phenomenon did not occur in cells directly exposed to arachidonic acid. Arachidonic acid has
404 been shown to exhibit potent pro-apoptotic effects on macrophages by causing cell cycle
405 arrest (Shen et al., 2018). In agreement, we observed a limited range in which macrophages
406 tolerated arachidonic acid (data not shown). Linoleic acid is the most highly consumed
407 polyunsaturated fatty acid found in the human diet. It is also the parent compound for the
408 family of ω6 polyunsaturated fatty acids including arachidonic acid, which is further converted
409 to a range of bioactive compounds such as leukotrienes, prostaglandins, and eicosanoids.
410 Together, this suggests that linoleic acid is the preferred pathway for arachidonic acid
411 expansion at the PI *sn*-2 position.

412 The activation of effector responses upon TLR ligation relies on signalling cascades involving
413 TIRAP/MyD88 or TRAM/TRIF adaptor molecules which activate NF-kB or IFN-dependent
414 signalling. Our data revealed that modified PI lipid chains elicit rapid degradation of the adaptor
415 protein TIRAP. Bound to PI(4,5)P2 -enriched plasma membrane regions or PI(3)P at the
416 endosomes, TIRAP surveys these compartments for activated TLRs. Notably, interaction with

417 PIPs at its N-terminal phosphoinositide-binding domain is critical for TIRAP membrane
418 recruitment and retention. A recent study demonstrated the participation of basic and nonpolar
419 residues in the TIRAP phosphoinositide-binding domain. Significantly, the authors found both
420 the inositol head group and acyl chains as critical in binding to TIRAP (Zhao et al., 2017).
421 Under conditions of reduced phosphoinositide binding, IRAK1/4 phosphorylated Thr28 residue
422 within the phosphoinositide-binding motif leading to TIRAP ubiquitination and degradation
423 (Zhao et al., 2017). Independently, another study demonstrated that the ratio of PIP2 to PIP3
424 at the plasma membrane influenced TLR signalling (Aksoy et al., 2012). A decrease in PIP2
425 abundance at the plasma membrane concurrently resulted in TLR4 internalization and TIRAP
426 redistribution to cytoplasmic compartments where it was degraded by the proteasome and
427 calpain. Altogether, it is tempting to speculate that the modified PI is either incompetent in
428 TIRAP binding and or fails to localize to the plasma membrane resulting in TIRAP
429 ubiquitination and degradation.

430 NLRP3 inflammasome is regulated both at the transcriptional and post-translational levels. In
431 particular, NLRP3 phosphorylation at distinct sites may either activate or inhibit the
432 inflammasome. We observed that the increased incorporation of long-chain arachidonic acid
433 by PI in WT cells through linoleic acid supplementation resulted in Ser293 phosphorylation in
434 the NACHT domain and dampened inflammasome activation. Previous studies have shown
435 increased phosphorylation at this site (Ser295) in THP-1 cells as a result of protein kinase A
436 activation by prostaglandin E2 (Mortimer et al., 2016). Considering that linoleic and
437 arachidonic acid are both precursors to prostaglandins, it may be interesting to test the overall
438 basal levels of prostaglandins in these cells. Nevertheless, our data reveal the regulation of
439 NLRP3 inflammasome by PI synthesis and metabolism at both the priming and activation
440 steps.

441 Immune signalling triggers an adjusted inflammatory response, and any overt activation of
442 these pathways may result in collateral damage. Therefore, it needs to be calibrated by
443 mechanisms that offer a variable degree of responses and are infallible. While the

444 phosphorylation of the inositol head group may at most result in seven distinct PIP species,
445 the possibility to add an array of fatty acids, with different carbon lengths and saturation status,
446 at the two positions on the PI glycerol linker offers far greater flexibility in terms of functions
447 the cellular PIs can serve. In conclusion, our study provides insights as to how changes in PI
448 lipid profile modify inflammasome activity and advances our understanding of the crosstalk
449 between lipid metabolism and immune signalling.

450

451 **Acknowledgements**

452 This work was supported in part by grants from The Wellcome Trust (108248/Z/15/Z), The
453 Medical Research Council, UK (MR/S00968X/1) and core funds from Imperial College London
454 to P.K.A. The authors declare no competing financial interests.

455

456 **Author Contributions**

457 C.H., A.O., S.C., G.L-M. and P.K.A. designed experiments; C.H., A.O., S.L., and K.M-R.
458 performed experiments; C.H., A.O., S.C., G.L-M. and P.K.A analyzed data; P.K.A. and G.L-
459 M. provided resources; P.K.A. wrote the original draft, and all authors approved the final
460 version. P.K.A provided overall supervision.

461

462 **Declaration of interests**

463 The authors declare that they have no conflict of interest.

464 **Figure Legends**

465 **Fig 1. ABC transporter B family member 1 is required for caspase-1 activation and IL-**
466 **1β secretion. (A)** Cell lysates from WT, *Abcb1b*$^{-/-}$ #1 and #2 cells were treated with or without
467 LPS (500 ng/ml) for 4 hours and immunoblotted for ABCB1 and GAPDH. **(B)** Relative ABCB1
468 protein levels in WT, *Abcb1b*$^{-/-}$ #1 and #2 cells measured with Image J on blots shown in (A).
469 **(C)** WT and *Abcb1b*$^{-/-}$ #1 and #2 cells were incubated with Rhodamine 123 (1 μM) for 30
470 minutes before measuring Rho123 accumulation on a fluorescent plate reader. **(D)** WT cells
471 without and with overnight exposure to U18666a (5 μg/ml) and control *Abcb1b*$^{-/-}$ cells grown
472 on coverslips were fixed in paraformaldehyde for 1 hour followed by overnight staining with
473 filipin (25 μg/ml) at 4 ^{o}C. Images were taken by confocal microscopy. **(E)** Total cholesterol
474 content in WT, *Abcb1b*$^{-/-}$ #1 and #2 cells measured by Amplex red assay. **(F)** WT, *Abcb1b*$^{-/-}$ #1
475 and *Abcb1b*$^{-/-}$ #2 cells were primed with LPS (500 ng/ml) for 4 hours followed by treatment with
476 either ATP (5 mM) or nigericin (20 nM) for approximately 45 minutes. Cell lysates were
477 collected and immunoblotted for caspase-1, GSDMD, and GAPDH. **(G)** Supernatants from
478 macrophages treated as in (F) were analysed for IL-1β secretion by ELISA. **(H)** Primary mouse
479 bone marrow-derived macrophages (BMDMs) were exposed to elacridar overnight (10 μM)
480 and incubated with Rhodamine 123 (1 μM) for 30 minutes to evaluate Rh123 accumulation as
481 in (C) above. **(I)** BMDMs were treated with increasing amounts of elacridar overnight (1, 2, 5
482 and 10 μM), followed by LPS priming (500 ng/ml) for 4 hours and nigericin (20 nM) for
483 approximately 45 minutes. Cell lysates were immunoblotted for caspase-1 and GAPDH. **(J)**
484 Supernatants from cells treated as in (I) were analysed for IL-1β secretion by ELISA. **(K)**
485 Immortalised BMDMs (iBMDMs) were treated with elacridar overnight (10 μM) followed by
486 LPS priming (500 ng/ml) for 4 hours and ATP (5 mM) for approximately 45 minutes. Cell
487 supernatants were analysed for IL-18 secretion by ELISA. Data shown are mean ± SD, and
488 the experiments shown are representative of at least three independent experiments. *, p =
489 <0.05; **, p = <0.01; ***, p = <0,001, ****, p = <0.0001, by Student's t-test.

490

491 **Fig 2. ABCB1 is required for the priming and activation of the NLRP3 inflammasome.**
492 **(A)** WT, *Abcb1b*$^{-/-}$ #1 and #2 cells primed with LPS (500 ng/ml) for 4 hours followed by
493 treatment with either ATP (5 mM) or nigericin (20 nM) for approximately 45 minutes. Cell
494 lysates were collected and immunoblotted for NLRP3, ASC, pro-IL-1β and GAPDH. **(B)** WT
495 and *Abcb1b*$^{-/-}$ #2 cells were stimulated with LPS (500 ng/ml) for the indicated time points. RNA
496 was extracted and converted into cDNA. Gene expression of *Nlrp3* and **(C)** *Il1β* was
497 determined by real-time PCR. **(D)** WT and *Abcb1b*$^{-/-}$ #2 cells were stimulated with LPS (500
498 ng/ml) for the indicated time points. Protein samples were collected and immunoblotted for
499 phospho-IκB, total IκB, phospho-p38 MAPK, total p38 MAPK and GAPDH. **(E)** Cells treated
500 as in B were examined for *Cxcl1 (KC)* and **(F)** *Tnfα* gene expression by real-time PCR. **(G)**
501 Supernatants from WT and *Abcb1b*$^{-/-}$ #2 macrophages treated as in (B) were analysed for
502 TNF-α cytokine secretion by ELISA. **(H)** WT and *Abcb1b*$^{-/-}$ #2 cells were stimulated with LPS
503 (500 ng/ml) for 4 hours and analysed for mRNA expression of *Ifnβ*. mRNA expression is shown
504 relative to *Gapdh.* **(I)** WT and *Abcb1b*$^{-/-}$ #2 cells were stimulated with either LPS (500 ng/ml),
505 Pam3 (1 μg/ml) or Imiquimod (1 μg/ml) for 4 hours and analysed for *Nlrp3* mRNA expression.
506 Gene expression is shown relative to *Gapdh*. Data shown are mean ± SD, and the
507 experiments shown are representative of 3 independent experiments. *, p = <0.05; **, p =
508 <0.01; ***, p = <0.001; ****, p = <0.0001, by Student's t-test.

509

510 **Fig 3. ABCB1 does not affect the activation of NLRC4 and AIM2 inflammasomes. (A)** WT
511 cells with or without exposure to elacridar (2, 5, 10 μM; 16 hours) and *Abcb1b*$^{-/-}$ #1 cells were
512 infected with *Salmonella typhimurium* at an MOI of 2 for approximately 4-5 hours. Cell lysates
513 were collected and immunoblotted for caspase-1, GSDMD and GAPDH. **(B)** WT, *Abcb1b*$^{-/-}$ *#1*,
514 and *Abcb1b*$^{-/-}$ #2 macrophages were infected with *Salmonella typhimurium* at an MOI of 2 for
515 approximately 4-5 hours and supernatants were analysed for IL-1β by ELISA. **(C)** Cells were
516 treated with LPS (500 ng/ml) for 4 hours followed by transfection with 1 μg of DNA complexed
517 to Lipofectamine 2000 (ratio DNA:Lipofectamine2000: 1:3) for approximately 4 hours to

518 activate the AIM2 inflammasome. Supernatants were analysed for IL-1β by ELISA. **(D)**
519 Supernatants from cells treated as in (B) and (C) or treated with LPS (500 ng/ml, 4 hours) and
520 ATP (5 mM, 45 minutes) were analysed for IL-18 production by ELISA. Data shown are mean
521 ± SD and is representative of at least three independent experiments. **, p=<0.01, *** p =
522 <0.001, **** p = <0.0001, by Student's t-test.

523

524 **Fig 4. Blunted NLRP3 inflammasome activation is associated with a shift in PI lipid**
525 **chains. (A)** Phosphatidylinositol structure consists of an inositol headgroup, a glycerol
526 backbone (red box), and two acyl chains R_1 and R_2 at the *sn-1* and *sn-2* positions (green
527 boxes). Representative spectra of **(B)** WT and **(C)** *Abcb1b*$^{-/-}$ cells. Peaks of interest are
528 indicated. The peaks at m/z 835.4, 861.4, 885.4 and 911.5 are assigned to phosphatidyl-
529 inositol (PI) 34:1, 36:2, 38:4 and 40:4, respectively. In this range are also found peaks at m/z
530 1354.7, m/z 1438.8 and m/z 1466.8, which are assigned to GM-2 d18:1/16:0, GM-2
531 d18:1/22:0, and GM-2 d18:1/C24:0 respectively. In the range m/z 1500-1650 are found GM-1
532 at m/z 1516.8, m/z 1544.8, m/z 1572.8, m/z 1600.9, m/z 1626.9 and m/z 1628.9 assigned to
533 GM-1 18:1/16:0, 18:1/18:0, 18:1/20:0, 18:1/22:0, 18:1/24:1 and 18:1/24:0, respectively. **(D)**
534 Ratio m/z of peaks 861/885 in WT and *Abcb1b*$^{-/-}$ macrophages. **(E)** Model showing PI
535 synthesis, and subsequent remodelling to acquire typical fatty acid configuration. WT and
536 *Abcb1b*$^{-/-}$ #2 cells were treated with LPS (500 ng/ml) for the indicated time points, and the
537 mRNA expression of **(F)** *Cds2*, **(G)** *Cdipt*, **(H)** *Lclat1*, and **(I)** *Lpiat* were analysed. Gene
538 expression is shown relative to *Gapdh*. Data shown are mean +/- SD and is representative of
539 at least three independent experiments. **, p=<0.01, *** p = <0.001, **** p = <0.0001, by
540 Student's t-test.

541

542 **Fig 5. Exogenous supplementation with linoleic acid alters PI acyl chain configuration.**
543 WT and *Abcb1*$^{-/-}$ cells were cultured in the presence of either arachidonic acid (5 μM, AA) or

544 AA (5 μM) and stearic acid (20 μM, SA) or linoleic acid (20 μM, LA) for at least two weeks with
545 the regular splitting of cell cultures every 2-3 days before subjecting the samples to whole-cell
546 lipidomics. **(A)** Ratio *m/z* of peaks 861/885 in cells grown in the presence of indicated fatty
547 acids. **(B-E)** WT cells cultured with the shown fatty acids were treated with LPS (500 ng/ml)
548 for the indicated time points, and the mRNA expression of **(B, D)** *Nlrp3*, and **(C, E)** *Il-1β* were
549 analysed. Gene expression is shown relative to *Gapdh*. **(F)** WT (and *Abcb1*$^{-/-}$) cells either
550 untreated or treated with MβCD (10 μm, 30 min) or the indicated fatty acids were stained with
551 cholera toxin B (CTB) (1 μg/mL) for 10 minutes at 4 °C followed by incubation with Alexa Fluor
552 488-conjugated anti-CTB antibody for 15 minutes at 4 °C to reveal GM1 presence.
553 Fluorescence was analysed by flow cytometry and representative spectra are shown. **(G)** MFI
554 (Mean fluorescence intensity) quantification of cells treated as above. Data shown are mean
555 ± SD and is representative of at least three independent experiments. *, p=<0.05, *** p =
556 <0.001, **** p = <0.0001, by Student's t-test.

557

558 **Fig 6. PI acyl chain profile regulates TIRAP expression. (A)** Control and LPS-primed WT
559 cells grown on coverslips were labelled with anti-TIRAP antibody and nuclei were stained with
560 DAPI. The plasma membrane was stained by adding AF-647-conjugated phalloidin for the last
561 15 min. **(B)** WT, *Abcb1*$^{-/-}$ and linoleic acid-supplemented cells were stimulated with LPS for
562 different times. Cell lysates were collected and immunoblotted for TIRAP and GAPDH. **(C)**
563 Quantitation of the WB shown in **(B)** by Image J. **(D)** WT and **(E)** linoleic acid-grown cells were
564 pre-treated or not with the proteasomal inhibitor MG132 (10 μM) for 30 min before stimulating
565 the cells with LPS for different time points. Cell lysates were collected and immunoblotted for
566 TIRAP and GAPDH. The data shown are representative of at least three independent
567 experiments. Asterisk (*) on immunoblots donates a non-specific band. Bars, 5 μm.

568

569 **Fig 7. Altered PI acyl chain profile blunts inflammasome activity by increasing NLRP3**
570 **phosphorylation. (A)** WT and linoleic acid-supplemented cells (LA) were either left untreated
571 or primed with LPS (500 ng/ml) for 4h followed by treatment with either ATP (5 mM) or nigericin
572 (20 nM) for approximately 45 minutes. Cell lysates were collected, and protein quantified. The
573 amount of protein loaded for linoleic acid -supplemented cells was increased to normalize total
574 NLRP3 levels. Cell lysates were immunoblotted for phosphor-NLRP3, total NLRP3, and ASC.
575 **(B)** Quantitative analysis of the WB shown in **(A)** by Image J**. (C)** Control WT, arachidonic
576 acid-grown cells (AA) and linoleic acid-grown cells (LA) were primed with LPS (500 ng/ml) for
577 4h followed by treatment with ATP (5 mM) for approximately 45 minutes. Caspase-Glo 1
578 activity was measured in the culture supernatants. **(D)** Cell supernatants collected as in **(A)**
579 were assayed for IL-18 secretion by ELISA. **(E)** WT, *Abcb1*$^{-/-}$, arachidonic acid-grown (AA) or
580 linoleic acid-grown cells (LA) cells were exposed to LPS + ATP followed by labelling with anti-
581 ASC antibody and DAPI staining. **(F)** Quantitative analysis of the percentage of cells with ASC
582 specks in samples treated as above. Each dot represents an individual field with at least n =
583 40 cells. Data shown are mean ± SEM, and the experiments shown are representative of at
584 least three independent experiments. Arrowheads show ASC specks. Bars, 5 µm. **, p=<0.01,
585 *** p = <0.001, **** p, = <0.0001 by Student's t-test.

586

587 **Fig 8. Schematic for ABCB1- and PI -mediated regulation of the NLRP3 inflammasome.**
588 ABCB1 is important in maintaining lipid metabolism. In the absence of ABCB1, the PI lipid
589 chain configuration is altered resulting in the reduced ratio of short-chain to long-chain fatty
590 acids. The activation of TLR4-dependent pathway relies on the adaptor protein TIRAP binding
591 to PIP2 for precise positioning at the plasma membrane. However, alteration in PI-lipid profile
592 results in at least two distinct outcomes which affect both the priming and activation steps of
593 the NLRP3 inflammasome. First, either due to inability to bind to PIP2 and or reduced PIP2
594 abundance at the PM, TIRAP is ubiquitinated and degraded in the cytoplasm. Inflammasome
595 assembly requires NLRP3, ASC, and pro-Caspase-1 in a complex wherein caspase-1

596 activation leads to the maturation of pro-IL-1β into the activation form. Altered PI profile most
597 likely increases PGE2 secretion because of increased PI incorporation of precursor
598 arachidonic acid. As a result, NLRP3 is phosphorylated at Ser293 residue which is mediated
599 by protein kinase A (PKA) leading to NLRP3 inactivation. Consequently, assembly of the
600 inflammasome is abrogated resulting in blunted caspase-1 activation and IL-1β secretion.
601 PGE2, prostaglandin E2; TIRAP, Toll-interleukin-1 receptor (TIR) domain-containing adaptor
602 protein; PIP2, phosphatidylinositol (4,5) bisphosphate.

603

604 **Materials and Methods**

605 **Ethics Statement**

606 Experiments involving animals were performed in accordance with the Animals (Scientific
607 Procedures) Act 1986, in accordance with a current UK Home Office licence and with approval
608 from the Imperial College Animal Welfare and Ethical Review Body (AWERB).

609 **Bone-marrow derived macrophage isolation and cell culture**

610 Bone marrow obtained from C57BL/6 mice (Charles River, UK) was isolated from the femurs
611 and tibias of 6-8 week old mice as previously described (Anand et al., 2012, 2011). Bone
612 marrow cells were then incubated in Dulbecco's Modified Eagle Medium (DMEM) containing
613 10% heat-inactivated fetal bovine serum (FBS), 1% penicillin/streptomycin, 1% HEPES, and
614 30% conditioned media from L929 fibroblasts for 5 to 6 days at 37 °C and 5% CO_2 for
615 macrophage differentiation. Wild-type (WT) immortalised BMDMs (iBMDMs) were kindly
616 provided by Katherine Fitzgerald and grown in DMEM containing 10% FBS, 1%
617 penicillin/streptomycin, 1% HEPES, and 10% L929 conditioned medium. Cells were incubated
618 and grown at 37 °C, 5% CO_2 and passaged every 2-3 days. HEK293T cells were grown in
619 DMEM containing % FBS and 1% HEPES at 37 °C, 5% CO_2. Cells were grown until confluent
620 and passaged every 2-3 days.

621 **Generation of CRISPR-Cas9 ABCB1b knock-out cells**

622 Guides targeted exon 10 and exon 11 of the *Abcb1b* gene were designed using the
623 CHOPCHOP online software (http://chopchop.cbu.uib.no/) and the Zhang Lab CRISPR
624 design software (http://crispr.mit.edu/). The guides contained a *BsmBI* overhang and were as
625 follows: Exon 10 gRNA – CACCGAAGCCTTTGCAAACGCACGA and its reverse complement
626 AAACTCGTGCGTTTGCAAAGGCTTC and exon 11 gRNA –
627 CACCGCCCATCGAGAAGCGAAGTTC and its reverse complement –
628 AAACGAACTTCGCTTCTCGATGGGC. Guide RNAs were annealed and ligated into the
629 LentiCRISPRv2 plasmid (Addgene #52961) at the *BsmBI* restriction site. The recombinant

630 plasmids (LentiCRISPRv2.gRNA10, LentiCRISPRv2.gRNA11) were then transformed into
631 competent *Escherichia coli (*NEB) according to the manufacturer's instructions. 1.85 µg of
632 LentiCRISPRv2gRNA10 plasmid or LentiCRISPRv2gRNA10 plasmid, 0.42ug pVSVg plasmid
633 and 1.3 µg psPAX2 plasmid were together transfected into the HEK923T cells using
634 polyethyleneimine (PEI; Sigma), at a ratio of 1 µg DNA: 3 µg PEI. Supernatants containing
635 lentiviral particles from transfected HEK293T cells were harvested at 48 hours post-
636 transfection. 300 µl of lentiviral particle-containing supernatant was then added to the iBMDMs
637 and cells were incubated at 37 °C for approximately 16 hours after which fresh media was
638 added to cells. Forty-eight hours following transduction, puromycin (6 µg/ml, Sigma) was
639 added for 7-10 days to select cells that had been successfully transduced. Puromycin-resistant
640 cells were then trypsinised and seeded into a 96-well plate at an approximate concentration
641 of 1 cell per well to obtain a clonal cell population. Single-cell colonies were identified and
642 expanded followed by Sanger sequencing to identify mutations in Exon 10 or 11 of the *Abcb1b*
643 gene. 2 clones, *Abcb1b*$^{-/-}$ #1 and #2 were identified with deletions of 32 and 9 base pairs in
644 exon 11, respectively (**Fig S2**).

645 **Cell stimulations**

646 Primary and immortalised macrophages were seeded into either 6-well plates at a
647 concentration of 2.5 x 10^6, 12 well plates at a concentration of 1 x 10^6 or 24-well plates at a
648 concentration of 0.5 x 10^6 cells per well. Where indicated, macrophages were treated with
649 elacridar (1-10 µM, SML0486 Sigma) or Ko143 (50–200 ng/ml, K2144, Sigma) for 16 hours.
650 In experiments with MβCD (C4555, Sigma), MβCD (5 – 10 µM) was added 30 minutes before
651 the addition of LPS. In experiments with MG132 (10 µM), it was added 30 minutes before the
652 addition of LPS. For fatty acid supplementation, distinct fatty acids were conjugated to albumin
653 as previously described (Hunt et al., 2004). Cells were continuously cultured with albumin-
654 bound arachidonic acid (5 µM), linoleic acid (20 µM), or a combination of arachidonic acid (5
655 µM) and stearic acid (20 µM) for at least two weeks prior to mass-spec analysis or any further
656 experiments.

657 **Inflammasome activation**

658 To activate the NLRP3 inflammasome, cells were incubated with LPS (500 ng/ml, Invivogen)
659 for 4-6 hours to prime the macrophages, followed by ATP (0.5 μM, Sigma) or Nigericin (20
660 nM, Tocris) for approximately 45 minutes. For NLRC4 inflammasome activation, the
661 *Salmonella Typhimurium* strain SL1344 was cultured overnight in 5 ml Luria-Bertani (LB) broth
662 at 37 °C and on a shaker at 220 rpm. The bacteria were then added to the indicated cells,
663 treated with or without elacridar (1 – 5 μM) or *Abcb1b*$^{-/-}$ cells, at an MOI of 2 and incubated for
664 approximately 4 hours. For AIM2 inflammasome activation, macrophages were transfected
665 with 1 μg of poly(dA:dT) (Invivogen) complexed with Lipofectamine 2000 at a 1:3 ratio
666 according to the manufacturer's instructions for approximately 4-5 hours.

667 **Cell signalling experiments**

668 The indicated cells were seeded into 6-well plates at a concentration of 2 x 10^6 cells per well
669 and incubated with elacridar (5 μM) overnight. The following morning media was replaced and
670 cells were stimulated with LPS (500 ng/ml) for the following time points: 0 (no LPS control),
671 0.5, 1, 2 and 4 hours. Supernatants were discarded from each well and the cells were
672 subsequently washed with PBS and cells were collected in RIPA buffer. Samples were
673 incubated on ice for approximately 30 minutes before being centrifuged at 15000X g for 15
674 minutes at 4°C to remove nuclei. The supernatant was collected, and the protein concentration
675 of each sample was measured using the BCA Protein Assay kit (Thermo Scientific #23227)
676 according to the manufacturer's instructions. Samples were all standardised to 1 μg/μl before
677 immunoblot analysis.

678 **Immunoblot analysis**

679 For immunoblot of phosphospecific antibodies, cells were collected in RIPA lysis buffer
680 containing both protease and phosphatase inhibitors (Roche) and standardised to 1 μg/μl as
681 mentioned above. Samples were boiled at 95 °C for 5 minutes before being resolved on 12%
682 SDS-PAGE gels. For immunoblotting of caspase-1, NLRP3, IL-1β, ASC, GSDMD and

683 GAPDH, lysates were collected in cell lysis buffer containing NP-40, DTT, and protease
684 inhibitors. Samples were boiled at 95 °C for approximately 20-30 minutes before being
685 resolved on 12% SDS-PAGE gels. SDS-PAGE gels were transferred to nitrocellulose
686 membranes (GE Life Sciences) and subsequently blocked in a 5% milk solution in TBS-Tween
687 (0.05%). Membranes were then incubated with the primary antibody overnight at 4 °C followed
688 by incubation with the HRP-conjugated secondary antibody at room temperature for 1 hour.
689 The primary antibodies used were as follows: P-glycoprotein (1:1000, Invitrogen MA1-2652),
690 Caspase-1 (1:2000, AdipoGen #AG-20B-0042-C100), NLRP3 (1:2000, AdipoGen #AG-20B-
691 0014-C100), ASC (1:2000, Adipogen #AG-25B-0006, AL177), GSDMD (1:1000, Abcam
692 #ab209845), IL-1β (1:500, Cell Signalling #12426), GAPDH (1:2500, ThermoFisher # MA5-
693 15738), Ikβα (1:1000, Cell Signalling, #9242), phosphor-IKβα (1:1000,Cell Signalling,
694 #2859S), p38 MAPK (1:1000, Cell Signalling, #9212), phospho-p38 MAKP (1:1000, Cell
695 Signalling, #4511), AKT (1:1,000; 4691; Cell Signaling Technology), phospho-AKT (1:1,000;
696 4060; Cell Signaling Technology), p70-S6K1 (1:1,000; 2708; Cell Signaling Technology),
697 phospho–p70-S6K1 (1:1,000; 9234; Cell Signaling Technology), TIRAP (1:1000;
698 Thermofisher; #PA5-88657), phospho-NLRP3 (1:1000, Thermofisher, # PA5-105071). The
699 HRP-conjugated secondary antibodies (ThermoFisher) were used at 1:5000. Following
700 secondary antibody incubation, proteins were visualised using either BioRad Clarity ECL
701 substrate (BioRad #1705060) or the Pierce ECL Western Blotting Substrate (Thermo Scientific
702 #32209) and processed on a Bio-Rad imager. Images were obtained using the Bio-Rad
703 software, ImageJ.

704 **ELISA**

705 Cell culture supernatants were measured for IL-1β (eBioscience #88-7013-88), TNF-α
706 (eBioscience #88-7324-88) and IL-18 (MBL #7625), using ELISA kits according to the
707 manufacturer's instructions.

708 **Real-time PCR**

709 RNA was isolated using TRIzol (Sigma # T9424) according to the manufacturer's instructions.
710 250 µg of RNA from each sample was then reverse transcribed into cDNA using the High-
711 capacity cDNA Reverse Transcription kit (Applied Biosystems #4368814) according to
712 manufacturer's instructions. Real-time PCR was then performed using the specific primers
713 detail in **Table 1**. Real-time PCR was performed on an ABI7500 or ABI7900HT (Applied
714 Biosystems) fast real-time PCR instrument.

715 Table 1

Gene	Forward Primer	Reverse Primer
Gapdh	CGTCCCGTAGACAAAATGGT	TTGATGGCAACAATCTCCAC
Nlrp3	TCACAACTCGCCCAAGGAGGAA	AAGAGACCACGGCAGAAGCTAG
Il1β	GATCCACACTCTCCAGCTGCA	CAACCAACAAGTGATATTCTCCATG
Tnfα	CATCTTCTCAAAATTCGAGTGACAA	TGGGAGTAGACAAGGTACAACCC
Kc	CAATGAGCTGCGCTGTCAGTG	CTTGGGGACACCTTTTAGCATC
Ifnβ	GCCTTTGCCATCCAAGAGATGC	ACACTGTCTGCTGGTGGAGTTC
Abcb1a	AACTCAGAGCCGCTTCTTCC	CTGTCCAGCCAACCTGCATA
Abcb1b	GGTGGTGTCATTGTGGAGCAAG	GCATCAGTGTCACTCTGGGATC
Abcg2	CAGTTCTCAGCAGCTCTTCGAC	TCCTCCAGAGATGCCACGGATA
Lpiat	TGCTATGGCACAGACTTCTGCG	ACTCAACAGCATGGTCCAGGCA
Lclat1	CCAGAAGGAACTGACCTCACAG	TCTCTTAGGCGGTCCACCACAA
Cdipt	GGACTCCTAGACGCTTTCGATG	CAGGTTGACCAAGAGACACATGG
Cds2	GGCTTCTTTGCCACTGTGGTGT	CCACAGTGAAGCTGTTGGTGTC

716

717 **Rhodamine 123 accumulation assay**

718 BMDMs or *Abcb1b*$^{-/-}$ clones were seeded into 96-well plates at a concentration of 1 x 10^5 cells
719 per well. Where indicated, BMDMs were treated with elacridar overnight (2-10 μM). Rho123
720 (2 μM, Sigma) was added and cells were incubated at 37 °C for 30 minutes. Cells were then
721 washed with PBS 3 times to remove any extracellular Rho123 and DMEM media was
722 replaced, after which cells were incubated for a further 30 minutes at 37 °C. Cells were then
723 washed again with PBS and lysed in cell lysis buffer before being read at excitation and
724 emission wavelengths of 485 and 535 nm, respectively in a fluorescent plate reader.

725 **Total cholesterol measurement**

726 Total cholesterol was measured using the Cholesterol Amplex Assay kit according to the
727 manufacturer's recommendations.

728 **Filipin staining**

729 WT and *Abcb1b*$^{-/-}$ cells were seeded onto coverslips at a concentration of 4 x 10^5 cells per
730 well. After they had adhered, cells were fixed in 4% paraformaldehyde for 1 hour at room
731 temperature. Cells were then stained with 25 μg/ml filipin (F9765, Sigma) overnight and
732 washed 3 times with PBS before mounting on glass slides. Images were visualised on a Leica
733 SP5 confocal microscope using 405 nm excitation and processed using the ImageJ
734 programme.

735 **GM1 staining**

736 Lipid rafts were assessed by specific labelling of endogenous GM1 ganglioside (a lipid raft
737 marker) with the Vybrant Alexa Fluor 488 Lipid Raft labelling kit which makes use of
738 fluorescently conjugated-CTB. The procedure was carried out according to the manufacturer's
739 instructions (Thermofisher). Samples were imaged using a Leica SP5 confocal microscope.
740 Flow cytometry was performed using the Attune NxT Flow Cytometer (Thermofisher) and
741 mean fluorescence intensity (MFI) was calculated using FlowJo™ v10.

742 **Caspase-1 inflammasome assay**

743 In some experiments, caspase-1 activity in the cell culture supernatants was measured using
744 Caspase-Glo® 1 inflammasome assay according to the manufacturer's instructions
745 (Promega). Luminescence was measured using an Omega plate reader.

746 **Immunofluorescence**

747 WT, *Abcb1b*$^{-/-}$ and linoleic acid -supplemented cells were seeded onto coverslips at a
748 concentration of 4 x 10^5 cells/well. After the experimental conditions, cells were fixed in 4%
749 paraformaldehyde for 1 hour at room temperature and washed twice with PBS-glycine
750 (50mM). The coverslips were blocked by incubating them for 20 minutes with PBS containing
751 1% BSA. Cells were then labelled with either anti-ASC antibody (1:100; AG-25B-0006, AL177;
752 AdipoGen) or anti-TIRAP antibody (1:100; Thermofisher; #PA5-88657) for 1h at room
753 temperature. Coverslips were then washed with PBS twice before incubating them with
754 secondary antibodies (Thermofisher). Actin staining was carried out by labelling samples with
755 Alexa Fluor™ 647 -conjugated phalloidin (Thermofisher; A22287) for 30 minutes. Coverslips
756 were washed 3 times and mounted on slides using Fluoromount-G™ mounting medium with
757 DAPI (Thermofisher; 00-4959-52). Images were acquired on an SP5 confocal microscope and
758 analysed using ImageJ software.

759 **MALDI-MS Analysis**

760 WT and *Abcb1b*$^{-/-}$ macrophages were cultured in DMEM before being trypsinised and
761 analysed via mass spectrometry. Prior to analysis, the super-2,5-dihydroxybenzoic acid
762 (Sigma-Aldrich, catalogue no. 50862) matrix was added at a concentration of 10 mg/mL in a
763 chloroform/methanol mixture at a 90:10 (v/v) ratio; 0.4 µL of a cell solution at a concentration
764 of 2 × 10^5 to 2 × 10^6 mL^{-1}, preliminary washed three times with double distilled water.
765 corresponding to ∼100–1000 cells per well of the MALDI target plate (384 Opti-TOF 123 mm
766 × 84 mm AB Sciex NC0318050, 1016629), and 0.8 µL of the matrix solution were deposited
767 on the MALDI target plate. These were then gently mixed with a micropipette, and left to dry.

768 MALDI-TOF MS analyses were performed on a 4800 Proteomics Analyzer (with TOF-TOF
769 Optics, Applied Biosystems) using the reflectron mode. Samples were analyzed in the
770 negative ion mode operating at 20 kV. A total of three independent experiments were
771 performed. Data obtained from mass-spec were analyzed using Data Explorer version 4.9
772 (Applied Biosystems), and assignments were based on the MS/MS fragmentation profile.

773 **Statistical Analysis**

774 GraphPad Prism 9.0 software was used for data analysis. Data are represented as mean ±
775 SD and are representative of experiments done at least three times. Statistical significance
776 was determined by unpaired Student's *t-test*; $p<0.05$ was considered statistically significant.

References

Aksoy E, Taboubi S, Torres D, Delbauve S, Hachani A, Whitehead MA, Pearce WP, Berenjeno-Martin I, Nock G, Filloux A, Beyaert R, Flamand V, Vanhaesebroeck B. 2012. The p110δ isoform of the kinase PI(3)K controls the subcellular compartmentalization of TLR4 signaling and protects from endotoxic shock. *Nat Immunol 2012 1311* **13**:1045–1054. doi:10.1038/ni.2426

Anand PK. 2020. Lipids, inflammasomes, metabolism, and disease. *Immunol Rev*. doi:10.1111/imr.12891

Anand PK, Subbarao Malireddi RK, Lukens JR, Vogel P, Bertin J, Lamkanfi M, Kanneganti T-D. 2012. NLRP6 negatively regulates innate immunity and host defence against bacterial pathogens. *Nature* **488**. doi:10.1038/nature11250

Anand PK, Tait SWG, Lamkanfi M, Amer AO, Nunez G, Pagès G, Pouysségur J, McGargill M a, Green DR, Kanneganti T-DD, Pages G, Pouyssegur J, McGargill M a, Green DR, Kanneganti T-DD. 2011. TLR2 and RIP2 pathways mediate autophagy of Listeria monocytogenes via extracellular signal-regulated kinase (ERK) activation. *J Biol Chem* **286**:42981–42991. doi:10.1074/jbc.M111.310599

Barneda D, Cosulich S, Stephens L, Hawkins P. 2019. How is the acyl chain composition of phosphoinositides created and does it matter? *Biochem Soc Trans* **47**:1291–1305. doi:10.1042/BST20190205

Barnett KC, Kagan JC. 2020. Lipids that directly regulate innate immune signal transduction. *Innate Immun* **26**:4–14. doi:10.1177/1753425919852695

Blunsom NJ, Cockcroft S. 2020. Phosphatidylinositol synthesis at the endoplasmic reticulum. *Biochim Biophys acta Mol cell Biol lipids* **1865**. doi:10.1016/j.bbalip.2019.05.015

Casares D, Escribá P V., Rosselló CA. 2019. Membrane Lipid Composition: Effect on Membrane and Organelle Structure, Function and Compartmentalization and

802 Therapeutic Avenues. *Int J Mol Sci* **20**. doi:10.3390/IJMS20092167

803 Castrillo A, Joseph SB, Vaidya SA, Haberland M, Fogelman AM, Cheng G, Tontonoz P. 2003.
804 Crosstalk between LXR and Toll-like receptor signaling mediates bacterial and viral
805 antagonism of cholesterol metabolism. *Mol Cell* **12**:805–816. doi:10.1016/S1097-
806 2765(03)00384-8

807 Chen J, Chen ZJ. 2018. PtdIns4P on dispersed trans-Golgi network mediates NLRP3
808 inflammasome activation. *Nature* **564**:71–76. doi:10.1038/s41586-018-0761-3

809 Dash RP, Jayachandra Babu R, Srinivas NR. 2017. Therapeutic Potential and Utility of
810 Elacridar with Respect to P-glycoprotein Inhibition: An Insight from the Published In Vitro,
811 Preclinical and Clinical Studies. *Eur J Drug Metab Pharmacokinet*. doi:10.1007/s13318-
812 017-0411-4

813 de la Roche M, Hamilton C, Mortensen R, Jeyaprakash AA, Ghosh S, Anand PK. 2018.
814 Trafficking of cholesterol to the ER is required for NLRP3 inflammasome activation. *J Cell*
815 *Biol* **217**:3560–3576. doi:10.1083/JCB.201709057

816 Dickson EJ, Hille B. 2019. Understanding phosphoinositides: rare, dynamic, and essential
817 membrane phospholipids. *Biochem J* **476**:1. doi:10.1042/BCJ20180022

818 Dunne A, Carpenter S, Brikos C, Gray P, Strelow A, Wesche H, Morrice N, O'Neill LAJ. 2010.
819 IRAK1 and IRAK4 Promote Phosphorylation, Ubiquitination, and Degradation of MyD88
820 Adaptor-like (Mal). *J Biol Chem* **285**:18276. doi:10.1074/JBC.M109.098137

821 Falkenburger BH, Jensen JB, Dickson EJ, Suh B-C, Hille B. 2010. Phosphoinositides: lipid
822 regulators of membrane proteins. *J Physiol* **588**:3179.
823 doi:10.1113/JPHYSIOL.2010.192153

824 Fernandis AZ, Wenk MR. 2007. Membrane lipids as signaling molecules. *Curr Opin Lipidol*.
825 doi:10.1097/MOL.0b013e328082e4d5

826 Forster S, Thumser AE, Hood SR, Plant N. 2012. Characterization of rhodamine-123 as a

827 tracer dye for use in in vitro drug transport assays. *PLoS One* **7**.
828 doi:10.1371/journal.pone.0033253

829 Garrigues A, Escargueil AE, Orlowski S. 2002. The multidrug transporter, P-glycoprotein,
830 actively mediates cholesterol redistribution in the cell membrane. *Proc Natl Acad Sci U*
831 *S A* **99**:10347–10352. doi:10.1073/pnas.162366399

832 Goud B, Picas L, Gaits-Iacovoni F. 2016. The emerging role of phosphoinositide clustering in
833 intracellular trafficking and signal transduction. *F1000Research* **5**:422.
834 doi:10.12688/f1000research.7537.1

835 Guo C, Chi Z, Jiang D, Xu T, Yu W, Wang Z, Chen S, Zhang L, Liu Q, Guo X, Zhang X, Li W,
836 Lu L, Wu Y, Song BL, Wang D. 2018. Cholesterol Homeostatic Regulator SCAP-SREBP2
837 Integrates NLRP3 Inflammasome Activation and Cholesterol Biosynthetic Signaling in
838 Macrophages. *Immunity*. doi:10.1016/j.immuni.2018.08.021

839 Hamilton C, Anand PK. 2019. Right place, right time: localisation and assembly of the NLRP3
840 inflammasome. *F1000Research* **8**. doi:10.12688/f1000research.18557.1

841 Hamilton C, Tan L, Miethke T, Anand PK. 2017. Immunity to uropathogens: The emerging
842 roles of inflammasomes. *Nat Rev Urol* **14**:284–295. doi:10.1038/nrurol.2017.25

843 He P, Gelissen IC, Ammit AJ. 2020. Regulation of ATP binding cassette transporter A1
844 (ABCA1) expression: Cholesterol-dependent and - Independent signaling pathways with
845 relevance to inflammatory lung disease. *Respir Res*. doi:10.1186/s12931-020-01515-9

846 Horton JD, Goldstein JL, Brown MS. 2002. SREBPs: activators of the complete program of
847 cholesterol and fatty acid synthesis in the liver. *J Clin Invest* **109**:1125–31.
848 doi:10.1172/JCI15593

849 Hunt AN, Skippen AJ, Koster G, Postle AD, Cockcroft S. 2004. Acyl chain-based molecular
850 selectivity for HL60 cellular phosphatidylinositol and of phosphatidylcholine by
851 phosphatidylinositol transfer protein α. *Biochim Biophys Acta - Mol Cell Biol Lipids*

852 **1686**:50–60. doi:10.1016/j.bbalip.2004.08.003

853 Kagan JC, Medzhitov R. 2006. Phosphoinositide-Mediated Adaptor Recruitment Controls Toll-
854 like Receptor Signaling. *Cell* **125**:943–955. doi:10.1016/j.cell.2006.03.047

855 Kalabis GM, Kostaki A, Andrews MH, Petropoulos S, Gibb W, Matthews SG. 2005. Multidrug
856 Resistance Phosphoglycoprotein (ABCB1) in the Mouse Placenta: Fetal Protection. *Biol*
857 *Reprod* **73**:591–597. doi:10.1095/BIOLREPROD.105.042242

858 Kaul D, Anand PK, Verma I. 2004. Cholesterol-sensor initiates M. tuberculosis entry into
859 human macrophages. *Mol Cell Biochem* **258**.
860 doi:10.1023/B:MCBI.0000012851.42642.be

861 Kawasaki T, Kawai T. 2014. Toll-like receptor signaling pathways. *Front Immunol* **5**:461.
862 doi:10.3389/fimmu.2014.00461

863 Kayagaki N, Stowe IB, Lee BL, O'Rourke K, Anderson K, Warming S, Cuellar T, Haley B,
864 Roose-Girma M, Phung QT, Liu PS, Lill JR, Li H, Wu J, Kummerfeld S, Zhang J, Lee WP,
865 Snipas SJ, Salvesen GS, Morris LX, Fitzgerald L, Zhang Y, Bertram EM, Goodnow CC,
866 Dixit VM. 2015. Caspase-11 cleaves gasdermin D for non-canonical inflammasome
867 signalling. *Nature* **526**:666–671. doi:10.1038/nature15541

868 Le Guédard M, Bessoule JJ, Boyer V, Ayciriex S, Velours G, Kulik W, Ejsing CS, Shevchenko
869 A, Coulon D, Lessire R, Testet E. 2009. PSI1 is responsible for the stearic acid
870 enrichment that is characteristic of phosphatidylinositol in yeast. *FEBS J* **276**:6412–6424.
871 doi:10.1111/j.1742-4658.2009.07355.x

872 Lopez-Castejon G, Luheshi NM, Compan V, High S, Whitehead RC, Flitsch S, Kirov A,
873 Prudovsky I, Swanton E, Brough D. 2013. Deubiquitinases regulate the activity of
874 caspase-1 and interleukin-1?? secretion via assembly of the inflammasome. *J Biol Chem*
875 **288**:2721–2733. doi:10.1074/jbc.M112.422238

876 Lupfer C, Anand PK. 2016. Integrating Inflammasome Signaling in Sexually Transmitted

877 Infections. *Trends Immunol* **37**:703–714. doi:10.1016/j.it.2016.08.004

878 Man SM, Kanneganti TD. 2015. Regulation of inflammasome activation. *Immunol Rev* **265**:6–
879 21. doi:10.1111/imr.12296

880 Mansell A, Smith R, Doyle SL, Gray P, Fenner JE, Crack PJ, Nicholson SE, Hilton DJ, O'Neill
881 LAJ, Hertzog PJ. 2006. Suppressor of cytokine signaling 1 negatively regulates Toll-like
882 receptor signaling by mediating Mal degradation. *Nat Immunol 2006 72* **7**:148–155.
883 doi:10.1038/ni1299

884 Mortimer L, Moreau F, MacDonald JA, Chadee K. 2016. NLRP3 inflammasome inhibition is
885 disrupted in a group of auto-inflammatory disease CAPS mutations. *Nat Immunol 2016*
886 *1710* **17**:1176–1186. doi:10.1038/ni.3538

887 Naguib A, Bencze G, Engle DD, Chio IIC, Herzka T, Watrud K, Bencze S, Tuveson DA, Pappin
888 DJ, Trotman LC. 2015. P53 mutations change phosphatidylinositol acyl chain
889 composition. *Cell Rep* **10**:8–19. doi:10.1016/j.celrep.2014.12.010

890 Romsicki Y, Sharom FJ. 2001. Phospholipid flippase activity of the reconstituted P-
891 glycoprotein multidrug transporter. *Biochemistry* **40**:6937–6947. doi:10.1021/bi0024456

892 Shen Z, Ma Y, Ji Z, Hao Y, Yan X, Zhong Y, Tang X, Ren W. 2018. Arachidonic acid induces
893 macrophage cell cycle arrest through the JNK signaling pathway. *Lipids Health Dis* **17**.
894 doi:10.1186/S12944-018-0673-0

895 Sonett J, Goldklang M, Sklepkiewicz P, Gerber A, Trischler J, Zelonina T, Westerterp M,
896 Lemaître V, Okada Y, D'Armiento J. 2018. A critical role for ABC transporters in persistent
897 lung inflammation in the development of emphysema after smoke exposure. *FASEB J*
898 **32**:6724–6736. doi:10.1096/fj.201701381

899 To KKW, Hu M, Tomlinson B. 2014. Expression and activity of ABCG2, but not ABCB1 or
900 OATP1B1, are associated with cholesterol levels: Evidence from in vitro and in vivo
901 experiments. *Pharmacogenomics* **15**:1091–1104. doi:10.2217/pgs.14.58

902 Traynor-Kaplan A, Kruse M, Dickson EJ, Dai G, Vivas O, Yu H, Whittington D, Hille B. 2017.
903 Fatty-acyl chain profiles of cellular phosphoinositides. *Biochim Biophys Acta* **1862**:513.
904 doi:10.1016/J.BBALIP.2017.02.002

905 Vaidyanathan A, Sawers L, Gannon A-L, Chakravarty P, Scott AL, Bray SE, Ferguson MJ,
906 Smith G. 2016. ABCB1 (MDR1) induction defines a common resistance mechanism in
907 paclitaxel- and olaparib-resistant ovarian cancer cells. *Br J Cancer 2016 1154* **115**:431–
908 441. doi:10.1038/bjc.2016.203

909 Van Meer G, Voelker DR, Feigenson GW. 2008. Membrane lipids: Where they are and how
910 they behave. *Nat Rev Mol Cell Biol*. doi:10.1038/nrm2330

911 Westerterp M, Gautier EL, Ganda A, Molusky MM, Wang W, Fotakis P, Wang N, Randolph
912 GJ, D'Agati VD, Yvan-Charvet L, Tall AR. 2017. Cholesterol Accumulation in Dendritic
913 Cells Links the Inflammasome to Acquired Immunity. *Cell Metab* **25**:1294-1304.e6.
914 doi:10.1016/j.cmet.2017.04.005

915 Yang J, Liu Z, Xiao TS. 2017. Post-translational regulation of inflammasomes. *Cell Mol*
916 *Immunol* **14**:65. doi:10.1038/CMI.2016.29

917 Yvan-Charvet L, Wang N, Tall AR. 2010. Role of HDL, ABCA1, and ABCG1 transporters in
918 cholesterol efflux and immune responses. *Arterioscler Thromb Vasc Biol*.
919 doi:10.1161/ATVBAHA.108.179283

920 Zhao X, Xiong W, Xiao S, Tang TX, Ellena JF, Armstrong GS, Finkielstein C V., Capelluto
921 DGS. 2017. Membrane targeting of TIRAP is negatively regulated by phosphorylation in
922 its phosphoinositide-binding motif. *Sci Rep* **7**:1–12. doi:10.1038/srep43043

923

924

925

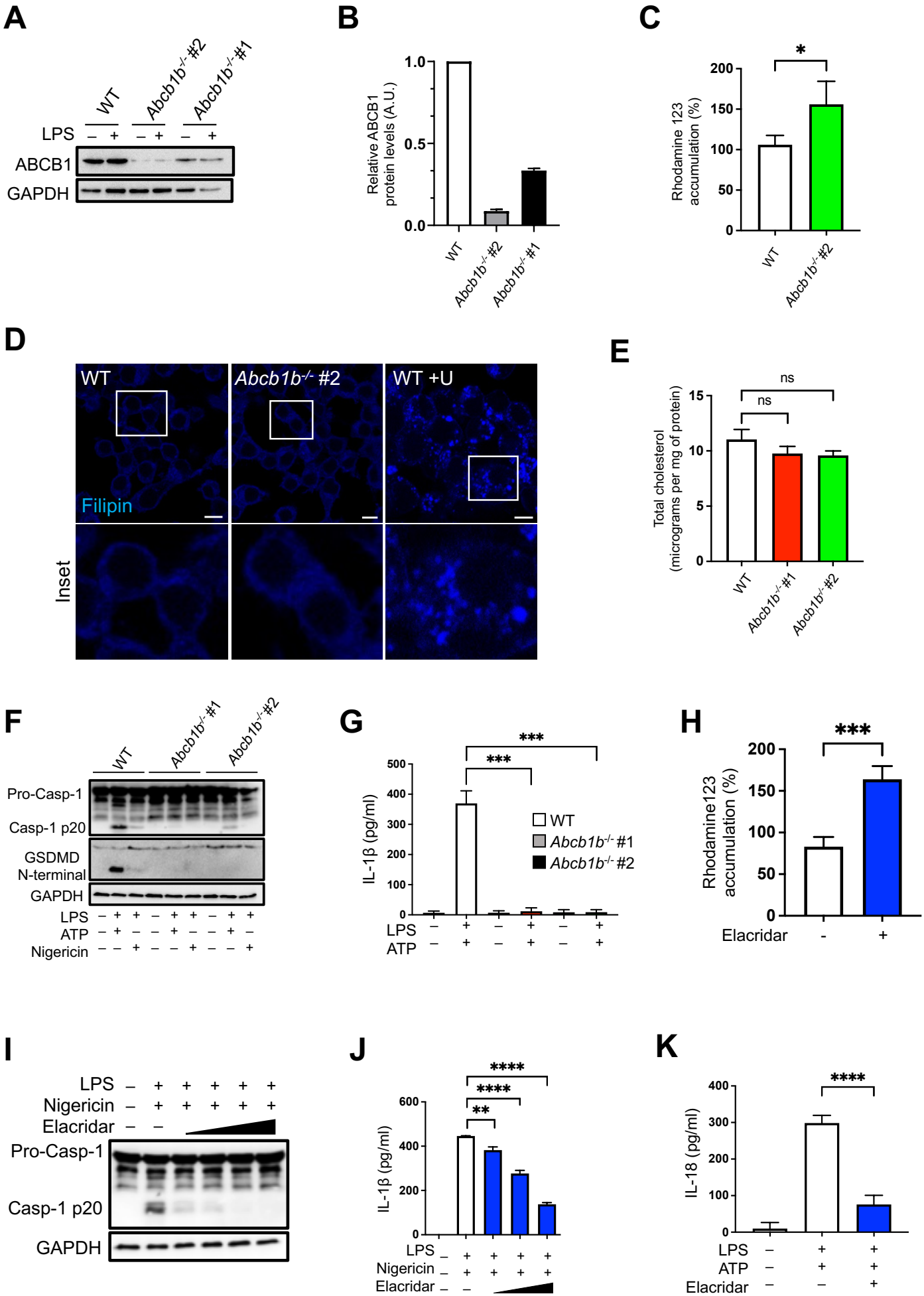
A
WT
Abcb1b-/- #2
Abcb1b-/- #1
LPS
ABCB1
GAPDH
B
Relative ABCB1 protein levels (A.U.)
1.0
0.5
0.0
WT
Abcb1b-/- #2
Abcb1b-/- #1
C
Rhodamine 123 accumulation (%)
200
150
100
50
0
*
WT
Abcb1b-/- #2
D
WT
Abcb1b-/- #2
WT +U
Filipin
Inset
E
Total cholesterol (micrograms per mg of protein)
15
10
5
0
ns
ns
WT
Abcb1b-/- #1
Abcb1b-/- #2
F
WT
Abcb1b-/- #1
Abcb1b-/- #2
Pro-Casp-1
Casp-1 p20
GSDMD N-terminal
GAPDH
LPS
ATP
Nigericin
G
IL-1β (pg/ml)
500
400
300
200
100
0
***
***
WT
Abcb1b-/- #1
Abcb1b-/- #2
LPS
ATP
H
Rhodamine123 accumulation (%)
200
150
100
50
0
***
Elacridar
-
+
I
LPS
Nigericin
Elacridar
Pro-Casp-1
Casp-1 p20
GAPDH
J
IL-1β (pg/ml)
600
400
200
0
****
****
**
LPS
Nigericin
Elacridar
K
IL-18 (pg/ml)
400
300
200
100
0
****
LPS
ATP
Elacridar

Figure 1

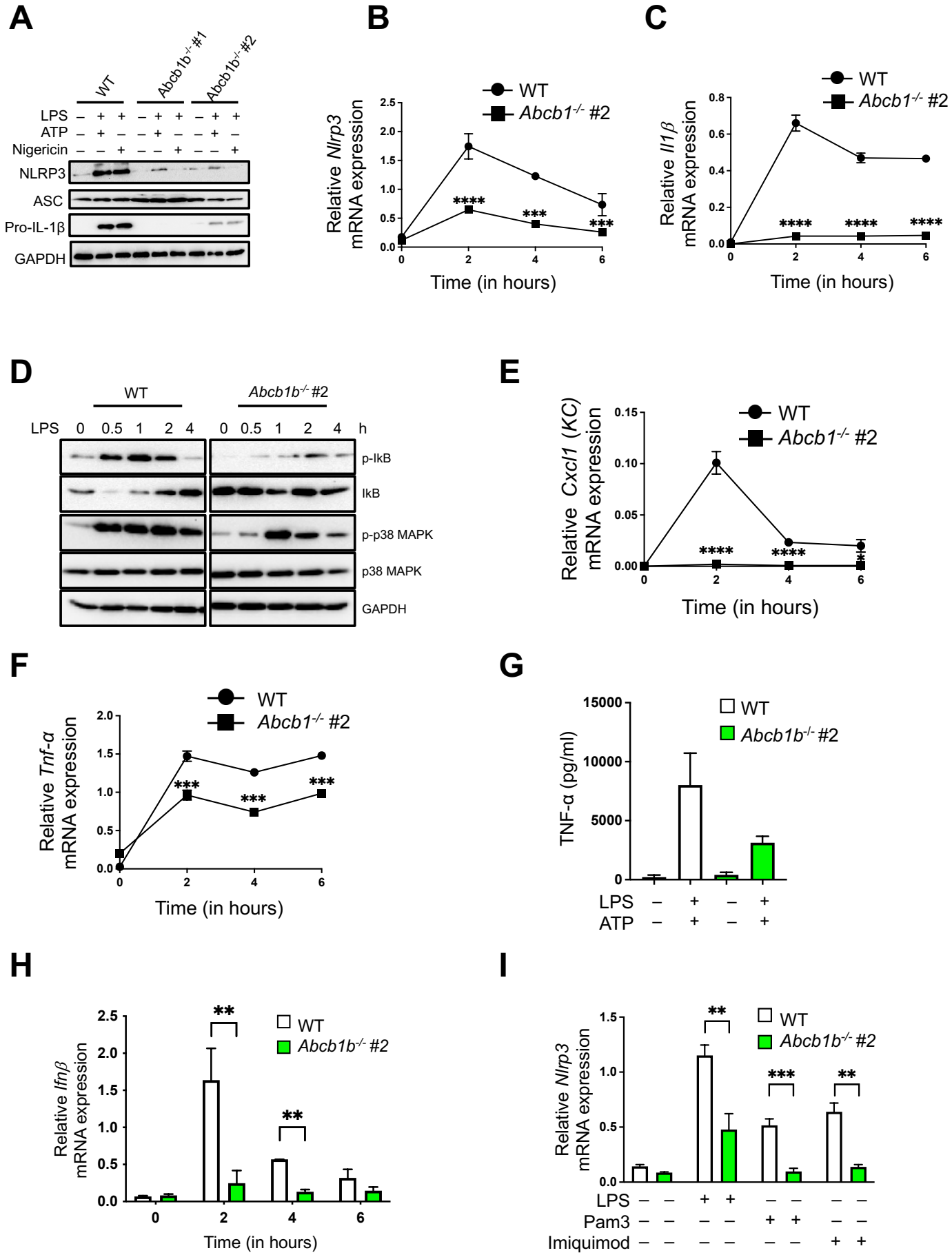
A
WT
Abcb1b-/- #1
Abcb1b-/- #2
LPS
ATP
Nigericin
NLRP3
ASC
Pro-IL-1β
GAPDH
B
WT
Abcb1-/- #2
Relative Nlrp3 mRNA expression
Time (in hours)
C
WT
Abcb1-/- #2
Relative Il1β mRNA expression
Time (in hours)
D
WT
Abcb1b-/- #2
LPS 0 0.5 1 2 4 0 0.5 1 2 4 h
p-IkB
IkB
p-p38 MAPK
p38 MAPK
GAPDH
E
WT
Abcb1-/- #2
Relative Cxcl1 (KC) mRNA expression
Time (in hours)
F
WT
Abcb1-/- #2
Relative Tnf-α mRNA expression
Time (in hours)
G
WT
Abcb1b-/- #2
TNF-α (pg/ml)
LPS
ATP
H
WT
Abcb1b-/- #2
Relative Ifnβ mRNA expression
Time (in hours)
I
WT
Abcb1b-/- #2
Relative Nlrp3 mRNA expression
LPS
Pam3
Imiquimod

Figure 2

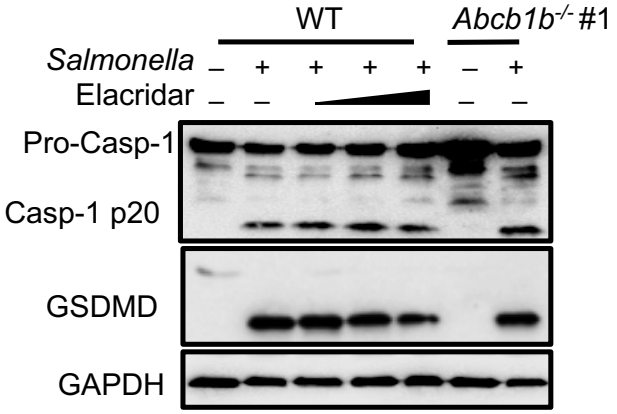
A
WT
Abcb1b-/- #1
Salmonella – + + + + – +
Elacridar – –
Pro-Casp-1
Casp-1 p20
GSDMD
GAPDH

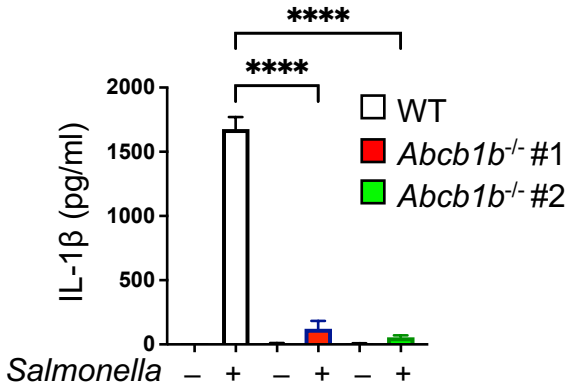
B
****
****
2000
1500
1000
500
0
IL-1β (pg/ml)
WT
Abcb1b-/- #1
Abcb1b-/- #2
Salmonella – + – + – +

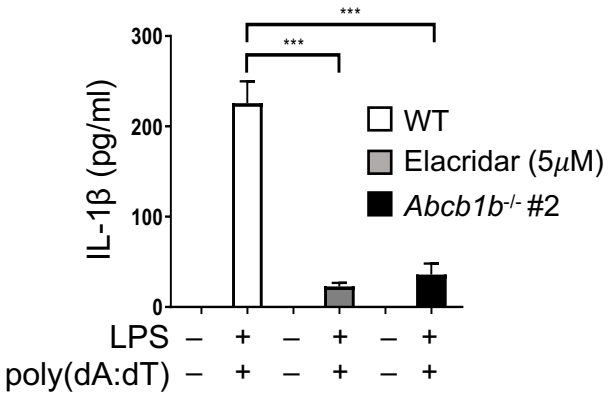
C
***
***
300
200
100
0
IL-1β (pg/ml)
WT
Elacridar (5μM)
Abcb1b-/- #2
LPS – + – + – +
poly(dA:dT) – + – + – +

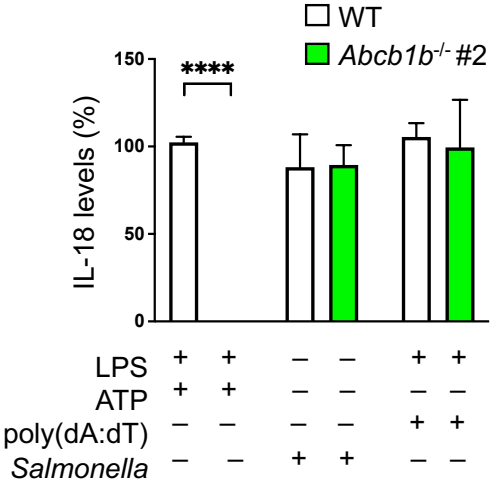
D
WT
Abcb1b-/- #2
****
150
100
50
0
IL-18 levels (%)
LPS + + – – + +
ATP + + – – – –
poly(dA:dT) – – – – + +
Salmonella – – + + – –

Figure 3

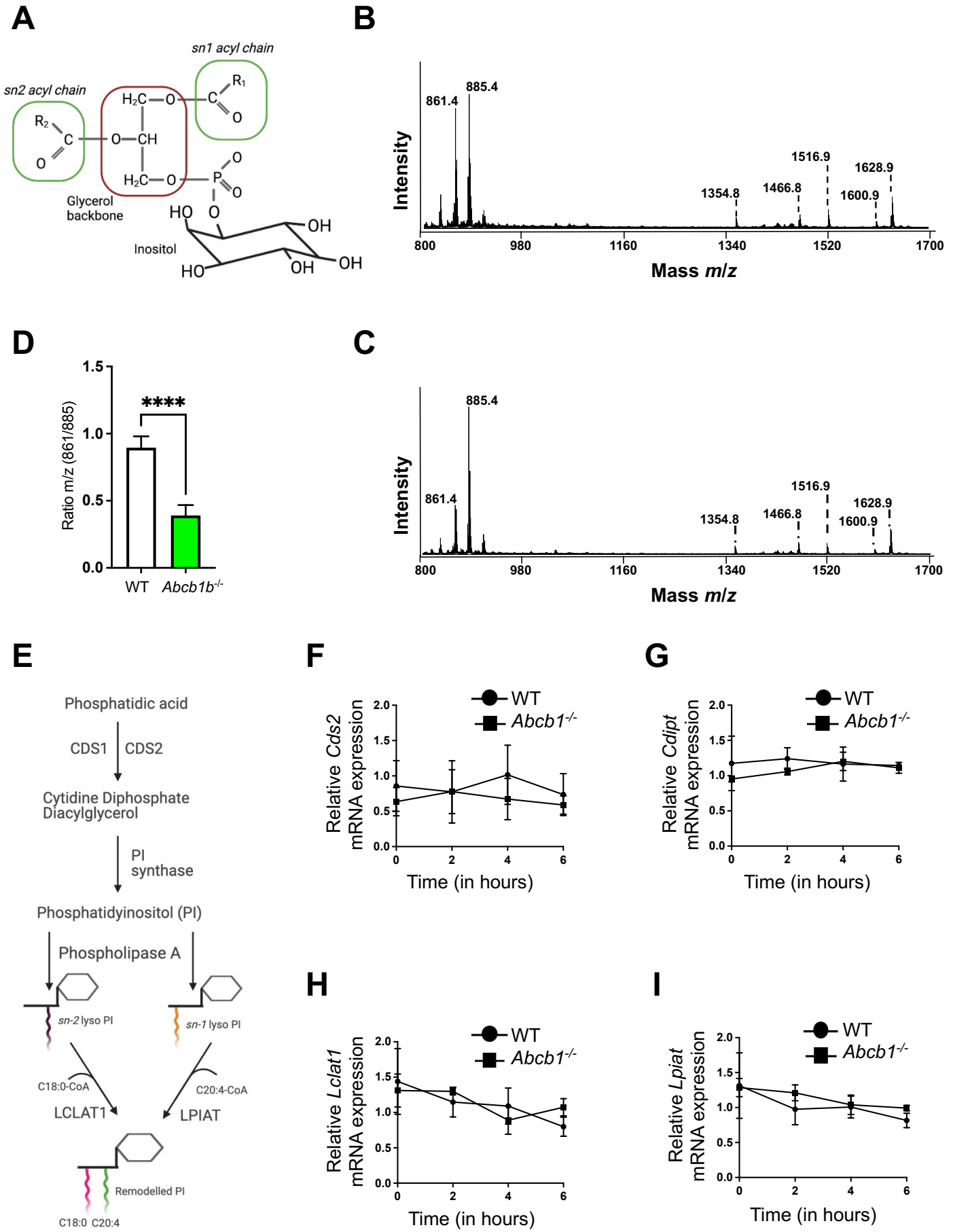
A
sn1 acyl chain
sn2 acyl chain
Glycerol backbone
Inositol
B
Intensity
Mass m/z
861.4
885.4
1354.8
1466.8
1516.9
1600.9
1628.9
D
Ratio m/z (861/885)
****
WT
Abcb1b-/-
C
E
Phosphatidic acid
CDS1
CDS2
Cytidine Diphosphate Diacylglycerol
PI synthase
Phosphatidyinositol (PI)
Phospholipase A
sn-2 lyso PI
sn-1 lyso PI
C18:0-CoA
C20:4-CoA
LCLAT1
LPIAT
Remodelled PI
C18:0 C20:4
F
Relative Cds2 mRNA expression
Time (in hours)
G
Relative Cdipt mRNA expression
H
Relative Lclat1 mRNA expression
I
Relative Lpiat mRNA expression

Figure 4

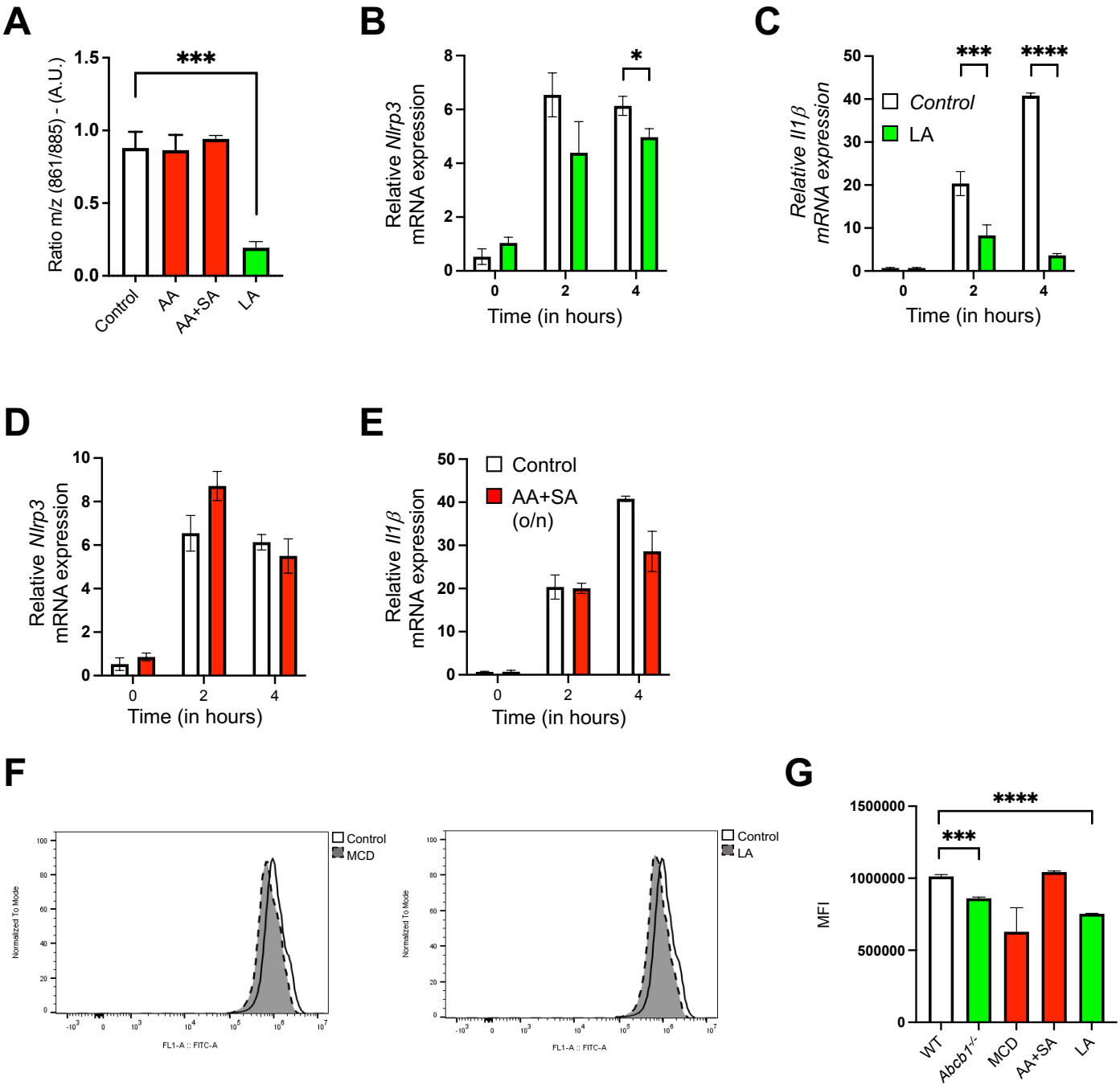
A
Ratio m/z (861/885) - (A.U.)
1.5
1.0
0.5
0.0
***
Control
AA
AA+SA
LA
B
Relative Nlrp3 mRNA expression
8
6
4
2
0
*
0
2
4
Time (in hours)
C
Relative Il1β mRNA expression
50
40
30
20
10
0
***
****
Control
LA
0
2
4
Time (in hours)
D
Relative Nlrp3 mRNA expression
10
8
6
4
2
0
0
2
4
Time (in hours)
E
Relative Il1β mRNA expression
50
40
30
20
10
0
Control
AA+SA (o/n)
0
2
4
Time (in hours)
F
Control
MCD
Normalized To Mode
FL1-A :: FITC-A
Control
LA
Normalized To Mode
FL1-A :: FITC-A
G
MFI
1500000
1000000
500000
0
****
***
WT
Abcb1-/-
MCD
AA+SA
LA

Figure 5

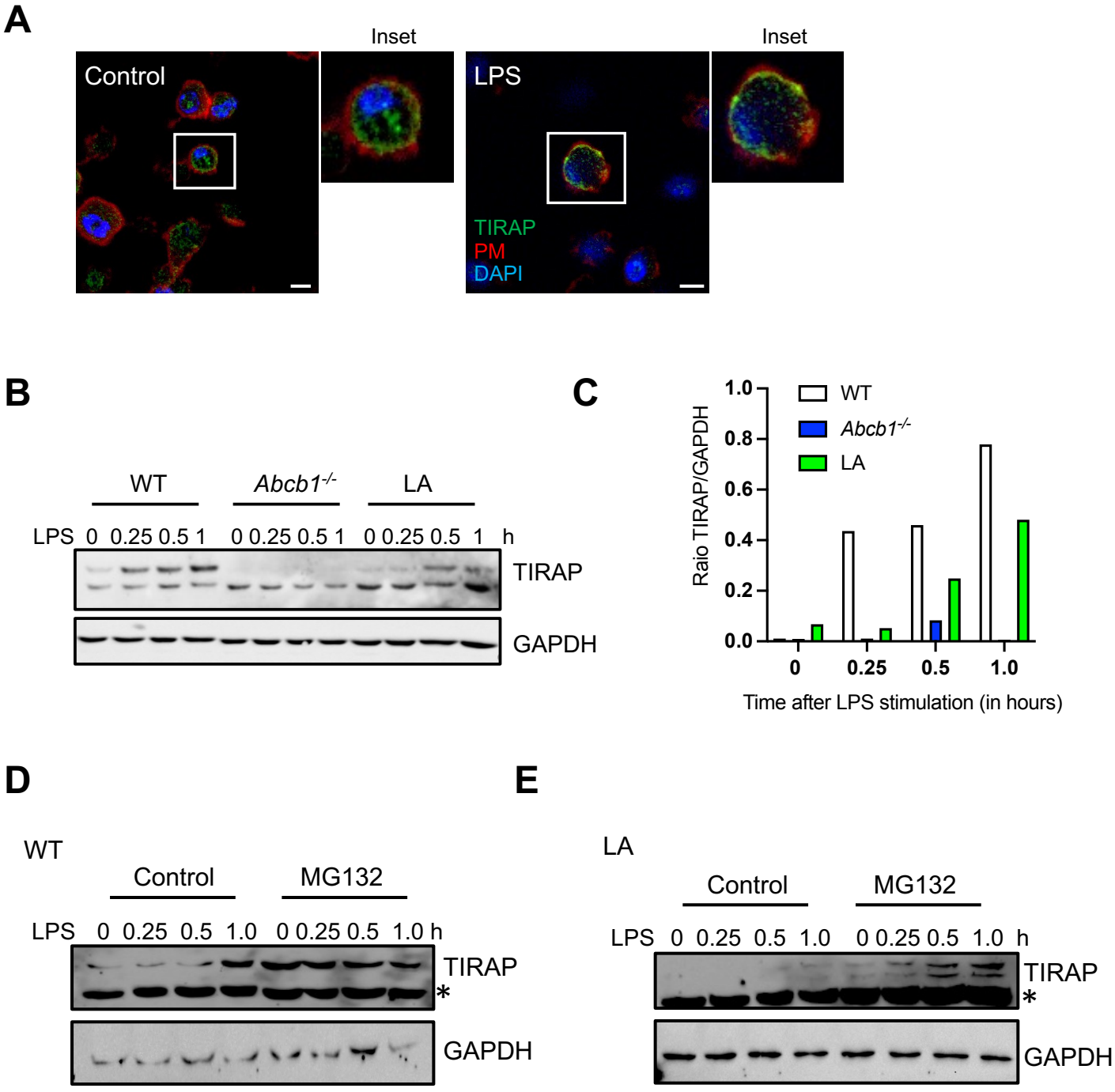
A
Inset
Inset
Control
LPS
TIRAP
PM
DAPI
B
WT
Abcb1-/-
LA
LPS 0 0.25 0.5 1 0 0.25 0.5 1 0 0.25 0.5 1 h
TIRAP
GAPDH
C
WT
Abcb1-/-
LA
Raio TIRAP/GAPDH
1.0
0.8
0.6
0.4
0.2
0.0
0
0.25
0.5
1.0
Time after LPS stimulation (in hours)
D
WT
Control
MG132
LPS 0 0.25 0.5 1.0 0 0.25 0.5 1.0 h
TIRAP
*
GAPDH
E
LA
Control
MG132
LPS 0 0.25 0.5 1.0 0 0.25 0.5 1.0 h
TIRAP
*
GAPDH

Figure 6

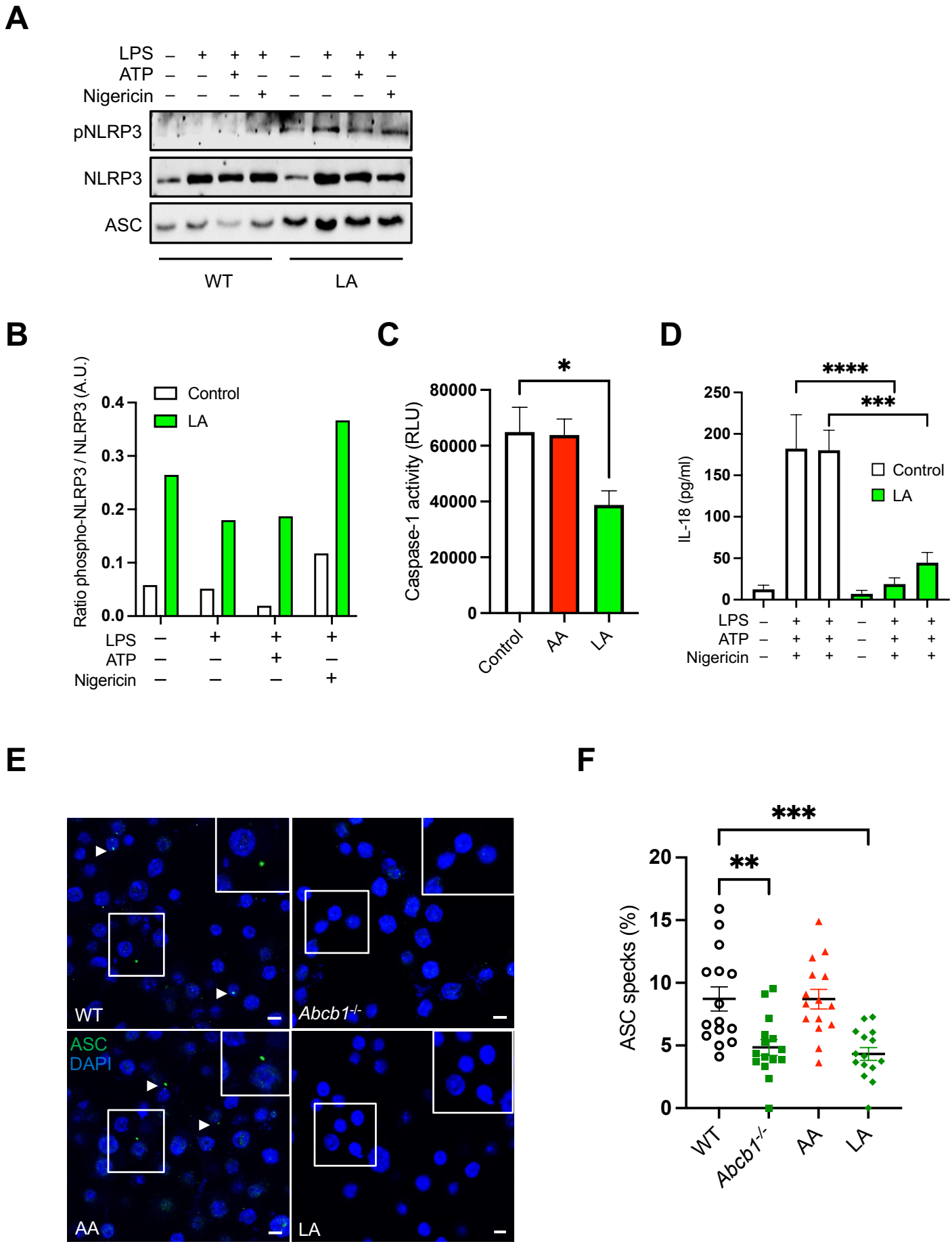
A
LPS
ATP
Nigericin
pNLRP3
NLRP3
ASC
WT
LA
B
Ratio phospho-NLRP3 / NLRP3 (A.U.)
Control
LA
C
Caspase-1 activity (RLU)
Control
AA
LA
D
IL-18 (pg/ml)
Control
LA
E
WT
Abcb1-/-
ASC
DAPI
AA
LA
F
ASC specks (%)
WT
Abcb1-/-
AA
LA

Figure 7

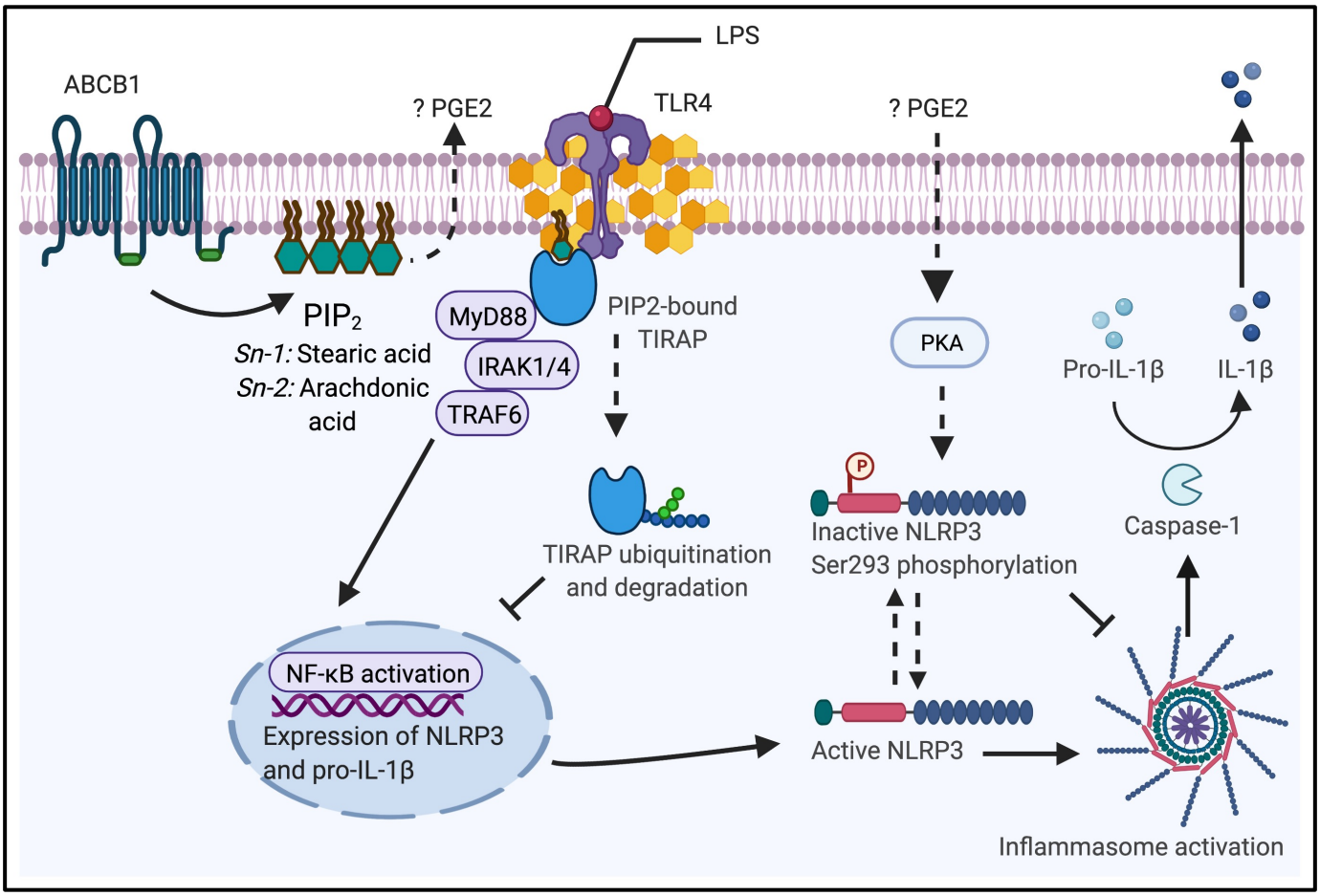
LPS
ABCB1
? PGE2
TLR4
? PGE2
PIP2
Sn-1: Stearic acid
Sn-2: Arachdonic acid
MyD88
IRAK1/4
TRAF6
PIP2-bound TIRAP
PKA
Pro-IL-1β
IL-1β
TIRAP ubiquitination and degradation
Inactive NLRP3
Ser293 phosphorylation
Caspase-1
NF-κB activation
Expression of NLRP3 and pro-IL-1β
Active NLRP3
Inflammasome activation

Figure 8